

1 **Orogenic lithosphere and slabs in the greater Alpine area - Interpretations based on teleseismic P-**
2 **wave tomography**

3
4 Mark R. Handy¹, Stefan M. Schmid², Marcel Paffrath³, Wolfgang Friederich³ and the AlpArray
5 Working Group^{*}

6
7 ¹ Institut für Geologische Wissenschaften, Freie Universität Berlin, Malteserstr. 74-100, 12249
8 Berlin, Germany; Institut für Geologie, ETH-Zürich, Sonneggstr. 5, 8092 Zürich

9 ² Institut für Geophysik, ETH-Zürich, Sonneggstr. 5, 8092 Zürich

10 ³ Institut für Geologie, Mineralogie, Geophysik, Ruhr-Universität Bochum, 44780 Bochum, Germany

11 ^{*}For the complete team list visit the link at the end of the paper

12
13
14

Deleted: of mantle structure in the Alps-Apennines-
Pannonian region frombased on

Deleted: V_p studies

18 **Abstract**

19 Based on recent results of AlpArray, we propose a new model of Alpine collision that involves
20 subduction and detachment of thick (~180 km) European lithosphere. Our approach combines
21 teleseismic P-wave tomography and existing Local Earthquake Tomography (LET) allowing us to
22 image the Alpine slabs and their connections with the overlying orogenic lithosphere at an
23 unprecedented resolution. The images call into question the conventional notion that downgoing
24 lithosphere and slabs comprise only seismically fast lithosphere. We propose that the European
25 lithosphere is heterogeneous, locally containing layered positive and negative V_p anomalies of up to
26 5-6%. We attribute this layered heterogeneity to seismic anisotropy and/or compositional
27 differences inherited from the Variscan and pre-Variscan orogenic cycles, rather than to thermal
28 anomalies. The lithosphere-asthenosphere boundary (LAB) of the European Plate therefore lies
29 below the conventionally defined seismological LAB. In contrast, the lithosphere of the Adriatic
30 Plate is thinner and has a lower boundary approximately at the base of strong positive V_p anomalies
31 at 100-120 km.

32 Horizontal and vertical tomographic slices reveal that beneath the Central and Western Alps, the
33 European slab dips steeply to the S and SE and is only locally still attached to the Alpine lithosphere.
34 However, in the Eastern Alps and Carpathians, this slab is completely detached from the orogenic
35 crust and dips steeply to the N-NE. This along-strike change in attachment coincides with an abrupt
36 decrease in Moho depth below the Tauern Window, the Moho being underlain by a pronounced
37 negative V_p anomaly that reaches eastward into the Pannonian Basin area. This negative V_p anomaly
38 is interpreted to represent hot upwelling asthenosphere that heated the overlying crust, allowing it
39 to accommodate Neogene orogen-parallel lateral extrusion and thinning of the ALCAPA tectonic
40 unit (upper plate crustal edifice of Alps and Carpathians) to the east. A European origin of the
41 northward-dipping, detached slab segment beneath the Eastern Alps is likely since its down-dip
42 length matches estimated Tertiary shortening in the Eastern Alps accommodated by originally
43 south-dipping subduction of European lithosphere.

44 A slab anomaly beneath the Dinarides is of Adriatic origin and dips to the northeast. There is no
45 evidence that this slab dips beneath the Alps. The slab anomaly beneath the northern Apennines,
46 also of Adriatic origin, hangs subvertically and is detached from the Apenninic orogenic crust and
47 foreland. Except for its northernmost segment where it locally overlies the southern end of the
48 European slab of the Alps, this slab is clearly separated from the latter by a broad zone of low V_p
49 velocities located south of the Alpine slab beneath the Po Basin. Considered as a whole, the slabs of
50 the Alpine chain are interpreted as highly attenuated, largely detached sheets of continental margin
51 and Alpine Tethyan oceanic lithosphere that locally reach down to a slab graveyard in the Mantle
52 Transition Zone (MTZ).

53

54

55 **1 Introduction**

56 The prevailing paradigm of mountain building in the greater Alpine area (Fig. 1) involves subduction
57 of European continental lithosphere that is some 100-120 km thick beneath the upper Adriatic
58 Plate, lithosphere thickness being based largely on seismological criteria (Jones et al., 2010; Geissler
59 et al., 2010, Kissling et al., 2006). We refer to this as the *standard lithosphere model* of continental
60 subduction to distinguish it from a new model here involving the subduction and partial
61 delamination of much thicker, compositionally heterogeneous European mantle. We base this
62 model on recent P-wave images of the AlpArray seismological campaign (Paffrath et al., 2021b)
63 presented below.

64 We use the terms *plate* and *slab* in a strictly structural-kinematic sense to refer to bodies of

Deleted: anomalously

Deleted: -200

Deleted: and

Deleted: suggest

Deleted: that

Deleted: the mantle of parts of the downgoing

Deleted: Plate

Deleted: is

Deleted: both

Deleted: ese

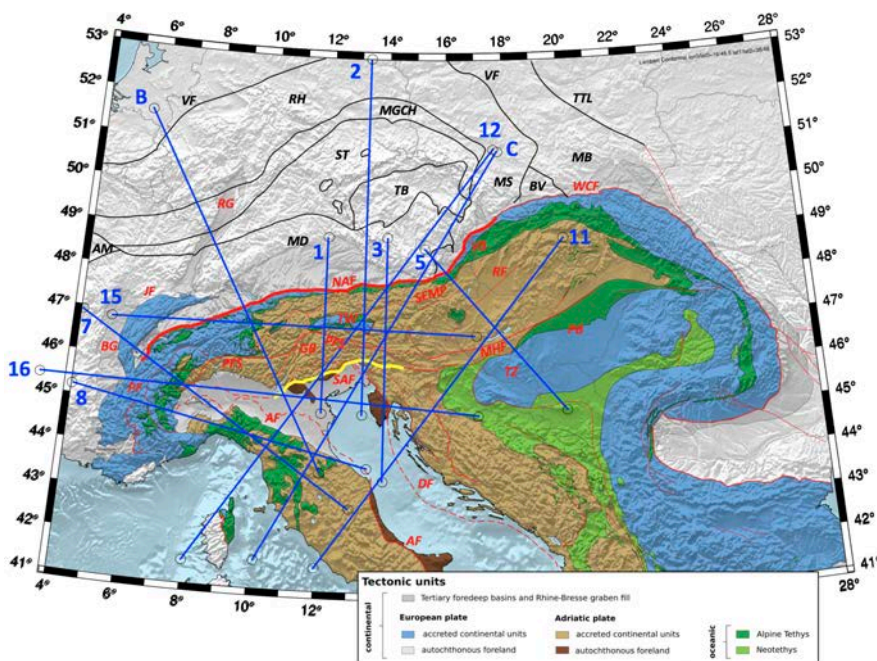
Deleted: (100-120 km)

Deleted: interface between

Deleted: and negative

Deleted: imaged

79 compositionally heterogeneous mantle and crust that have moved coherently with respect to
 80 markers in both the mantle and at the surface. As pointed out by Artemieva (2011), different
 81 geophysical techniques have given rise to a multitude of definitions of the lithosphere based on
 82 seismic, thermal, electrical, rheological, and petrological properties. Our definition therefore differs
 83 from strictly seismological definitions, which treat plates as seismically fast mantle lithosphere (e.g.,
 84 Piromallo & Morelli, 2003; Wortel & Spakman, 2000). Implicit in the structural-kinematic definition
 85 of lithosphere we use is that the base of the lithosphere is a shear zone that accommodates the
 86 relative motion of plates.
 87



88 **Figure 1:** Tectonic map of the Alpine chain and its foreland, including Variscan units. Thin red lines – main Tertiary
 89 tectonic faults after Schmid et al. (2004) and (2008); Thin black lines – tectonic lineaments separating Variscan
 90 tectonometamorphic domains after Franke (2017, 2000), Mazur et al. (2020), and Schulmann et al. (2014). Blue
 91 lines are traces of vertical tomographic profiles in Figs. 3-7. The numbers of the traces are in accordance with their
 92 appearance in Appendix A. Thick red line along the NAF marks the Oligo-Miocene plate boundary in the Alps;
 93 Yellow line along the SAF marks the presently active plate boundary in the Alps; Green units are the Adria-Europe
 94 suture marking the Late Cretaceous-to-late Eocene plate boundary.
 95 **Alpine faults and related structures:** NAF - North Alpine Front, SAF – Southern Alps Front; PFS - Periadriatic Fault
 96 System, GB – Giudicarie Belt, JF – Jura Front, PF – Penninic Front, RG – Rhein Graben, BG – Bresse Graben, TW –
 97 Tauern Window, SEMP – Salzach-Ennstal –Mariazell-Puch Fault, MHF – Mid-Hungarian Fault Zone, VB – Vienna
 98 Basin, PB – Pannonian Basin, RF – Raba Fault, WCF – Western Carpathian Front, DF – Dinaric Front
 99 **Variscan tectonic domains and faults:** VF – Variscan orogenic front, RH – Rheno-Hercynian, MGCH – Mid-German
 100 Crystalline High, ST – Saxo-Thuringian, MD – Moldanubian, TB – Tepla-Barrandian, AM – Armorican Massif, BV –
 101 Bruno-Vistulian, MB – Malopolska Block, MS – Moravo-Silesian. Other faults: TTL - Teyseyre-Thornquist Line
 102
 103

104 As in other orogenic belts, the standard model of lithospheric subduction in the Alps was
105 initially supported by teleseismic body-wave studies showing fast seismic velocity anomalies dipping
106 beneath the Alpine-Mediterranean mountain belts (Wortel and Spakman, 2000). They are often
107 inclined in the same direction as the dipping Mohos that define the base of the orogenic crust
108 (Waldhauser et al., 2002; Lippitsch et al., 2003; Spada et al., 2013). These seismically fast domains
109 are inferred to reflect negative temperature anomalies that mark descending slabs of cold
110 subcontinental lithospheric mantle, whereas positive anomalies at the base of, and surrounding,
111 these seismically fast domains are often interpreted as warm asthenospheric mantle (e.g., Spakman
112 and Wortel, 2004). In the Alps, the base of the subducting European Plate has thus been taken to be
113 the boundary between seismically fast and slow domains (respectively, blue and red domains in
114 most tomographic slices), whereas its top is the interface with the upper Adriatic Plate.
115 Seismological studies in the Western Alps have shown that this interface includes subducted crust
116 down to depths of > 90 km (Lippitsch et al., 2003; Zhao et al., 2015, 2016), corroborating geological
117 evidence of deeply subducted and exhumed fragments of oceanic and continental crust (e.g.,
118 Chopin, 1984; Schertl et al., 1991) and mantle (Brenker and Brey, 1997) preserved in the Alps (Agard
119 and Handy, 2021).

120 When assessing the geometry of subduction and plate boundaries in the Alps, it is important
121 to distinguish the Late Cretaceous-Paleogene Adria-Europe subduction plate boundary represented
122 by the Tethyan ophiolite belt along the Alps (Fig. 1) from the Oligo-Miocene collisional boundary
123 exposed along the Northern Alpine Front (labeled NAF in Fig. 1). Both of these boundaries differ
124 from the Pliocene-to-active plate boundary along the Southern Alpine Front (SAF in Fig. 1). In the
125 analysis below, these differently aged boundaries provide important kinematic and time constraints
126 for the tectonic interpretation of mantle anomalies. None of these geological boundaries coincide at
127 the surface, nor are they expected to merge at depth given that the Alps have experience changes
128 in the amount and direction of shortening with time (Schmid et al., 2004; Handy et al., 2010). This is
129 especially true of the eastern part of the Alps, where Paleogene N-S shortening and subduction has
130 given way to Mio-Pliocene eastward lateral extrusion of orogenic crust and possibly upper mantle
131 (e.g., Ratschbacher et al., 1991) that is still ongoing during continued Adria-Europe N-S convergence
132 (e.g., Grenerzcy et al., 2005; Serpelloni et al., 2016).

133 Controversy on Alpine subduction has arisen because the SE dip of the Alpine slab anomaly
134 in the Central and Western Alps (Lippitsch et al., 2003; Zhao et al., 2015, Lyu et al. 2017) indicating
135 "classical" SE-directed subduction of the European slab (e.g., Argand, 1924; Pfiffner et al., 1997;
136 Schmid et al., 1996) contrasts with a dip to the NE of a positive V_p slab anomaly in the eastern part
137 of the chain, i.e., east of 12-13°E in Fig. 1 (Lippitsch et al., 2003; Mitterbauer et al., 2011; Karousová
138 et al., 2013, Zhao et al. 2016). This NE dip is inconsistent with SE-directed Alpine subduction inferred
139 from the uniformly S-dip and N- to NW-directed shear sense indicators of sutured oceanic
140 lithosphere and crustal nappes all along the Alps (e.g., Schmid et al., 2004), including the Eastern
141 Alps (e.g., Handy et al., 2010 and refs. therein). The plate tectonic affinity of this part of the slab
142 beneath the Eastern Alps therefore remains unclear and debated. Proponents of a European origin
143 propose the existence of a very steeply NE-dipping overturned to subvertically oriented slab that
144 detached from the crust east of the Tauern Window (Mitterbauer et al., 2011; Rosenberg et al.,
145 2018). Proponents of an Adriatic origin of this slab based their interpretation on the tomographic
146 images of Lippitsch et al. (2013; their Fig. 13c) that depict a moderately NE-dipping slab still
147 attached to the still undeformed parts of the Adriatic Plate. They therefore proposed a late-stage
148 reversal of subduction polarity (Schmid et al., 2004; Kissling et al., 2006; Handy et al., 2015). A
149 recent review by Kästle et al. (2020) that also takes surface wave tomography into consideration

Deleted: n

Deleted: orogenic

Deleted: f

153 considers the possibility that this slab has a combined European-Adriatic origin, as discussed in
154 Handy et al. (2015).

155 In this paper, we interpret vertical and horizontal tomographic slices of the Alps generated by
156 integrating crustal and mantle tomographic P-wave models gleaned from the AlpArray seismological
157 network (Hetényi et al., 2018). This new method, described in the next section and in detail in
158 Paffrath et al. (2021b), employs teleseismic tomography and integrates the crustal/uppermost
159 mantle models of Diehl et al. (2009) and Tesauro et al. (2008) as *a priori* information into the
160 teleseismic inversion, weighted according to its reliability. This allows us to image the Alpine slabs
161 and their potential connections with the orogenic edifice as well as the fore- and hinterland
162 lithospheres at an unprecedented resolution. The images presented in sections 3 and 4 call into
163 question the conventional notion based on seismological criteria that slabs comprise only
164 seismically fast mantle lithosphere that is some 100-120 km thick. Instead, they suggest that the
165 down-going European Plate in the Alps is much thicker and contains positive and negative seismic
166 anomalies inherited from pre-Alpine (Variscan) events that, given their age, are likely to be of
167 structural and compositional, rather than thermal nature. In section 5, we showcase evidence for
168 large-scale delamination of the slabs in the Alps and northern Apennines, with slabs that have been
169 partly to entirely detached from their orogenic edifices. The discussion in section 6 revisits the
170 debate on subduction polarity in light of the new data and touches on some implications of
171 widespread delamination and slab detachment for crustal seismicity and foreland basin evolution.
172 We conclude with a conceptual 3-D visualization of mantle structure beneath the Alps and
173 Apennines that serves as a vehicle for assessing the interaction of slabs and asthenosphere at
174 depths down to the Mantle Transition Zone (MTZ).

175
176

177 2. Methodology

178 The images of velocity anomalies in this paper are derived from a 3D-model of P-wave velocity in
179 the crust and mantle below the greater Alpine region (Paffrath et al., 2021b). This is obtained by
180 tomographic inversion of teleseismic P-wave travel-time residuals measured on records of the
181 AlpArray Seismic Network (Paffrath et al., 2021a). Travel time residual is the difference between the
182 observed and a theoretical travel time calculated for a standard earth model. Calculation of the
183 travel-time residuals and the inversion procedure are described here in turn, as outlined in Paffrath
184 et al. (2021b, their chapt. 2 and Appendix A1).

185 The travel-time database comprises 162366 onsets of 331 teleseismic earthquakes of
186 magnitude 5.5 or higher at epicentral distances between 35 and 135 degrees occurring between
187 January 2015 and July 2019. Paffrath et al. (2021b) subtracted the array average from these
188 residuals on an event-to-event basis. This procedure avoids errors in earthquake origin time and
189 reduces influences of heterogeneities in earth structure outside the inversion domain (see Paffrath
190 et al., 2021a on obtaining highly accurate travel-time residuals suitable for teleseismic inversion).

191 Inversion of the travel-time residuals to obtain the P-wave velocity perturbations in the
192 depth slices and profiles of V_p anomalies below is a complex process. The aim of inversion is to find
193 a model that reduces the misfit between the observations and predictions of travel times to a
194 certain threshold value. Iteration of the inversion ends if either the observations fit within their
195 uncertainties or if the misfit reduction stagnates when executing further iterations.

196 Because teleseismic waves propagate subvertically through the crust, the resolution of
197 strongly heterogeneous crust is poor. Correcting for heterogeneities requires a velocity model of
198 the crust, termed an *a priori* model (e.g., Kissling, 1993), which is based on independent data, e.g.,
199 reflection and refraction seismics, receiver functions, local earthquake tomography. The standard

Deleted:

Deleted: that

202 correction method involves computing travel-time residuals for the crustal model on the
203 assumption of idealized wave fronts, then subtracting these residuals from the observed residuals.
204 This oversimplifies the true ray paths, which are refracted in the crust and underlying mantle
205 depending on vertical and azimuthal incidence.

206 The novel approach of Paffrath et al. (2012b) entails creating a starting model for inversion
207 iteration by superposing a 1-D standard earth model (here taken to be model AK135 of Kennett et
208 al., 1995) and a 3-D *a priori* model of the crust and uppermost mantle, then damping the inversion
209 according to the reliability of the *a priori* model (see below and Paffrath et al., 2021b on inversion
210 regularisation). The purpose of the *a priori* model is to account for strongly heterogeneous velocity
211 structure, particularly in the crust. In constructing their *a priori* crustal model, Paffrath et al. (2021b)
212 discretize the EuCRUST-07 model of Tesauro et al. (2008) and the fully three-dimensional, high-
213 resolution P-wave velocity model of Diehl et al. (2009) for the central Alpine region. In addition,
214 information on Moho depth in the Alpine region is refined using the study of Spada et al. (2013).

215 The P-wave velocity at a given point in the *a priori* model is a weighted average of the Diehl
216 and Tesauro models, with weights depending on the reliability of Diehl's model as measured by the
217 values of the diagonal elements of the resolution matrix (RDE). For values of RDE above 0.15 the
218 crustal model is dominated by Diehl's model, whereas for values below, the model of Tesauro et al.
219 (2008) takes over smoothly (see Paffrath et al. 2001b, their Fig. 2 for the areas in which these
220 models dominate). For regions of the inversion domain beyond the extent of the *a priori* crustal
221 model, Paffrath et al. (2021b) assume the modified standard earth model AK135 of Kennett et al.
222 (1995) and the 1D-reference model used by Diehl et al. (2009). The advantage of this multifaceted
223 approach is that it provides a comprehensive model of crust and mantle structure that allows for
224 refined interpretation of the orogenic crust and its transition to the underlying mantle lithosphere,
225 including subducted slabs.

226 Paffrath et al. (2021b) assess the resolution of mantle structures imaged in this study by
227 employing different general tests, as well as very specific resolution tests that focus on crucial,
228 smaller scale structures in the Alps, e.g., gaps and different dip directions of slabs. Among the general
229 tests are two checkerboard tests which regularly alter the velocity of the mantle in a synthetic model
230 by applying a perturbation of +/- 10% in P-wave velocity on different cell sizes of 2 x 2 x 3 grid points
231 and 3 x 3 x 4 grid points (Fig. 7 in Paffrath et al. 2021b). Gaps between the cells remain unperturbed
232 in order to analyse smearing throughout the irradiated model domain.

233 Checkerboard tests show that, due to the uneven event distribution, smearing is more
234 prominent in the NW-SE direction (Paffrath et al. 2021b, their Figs. 8-9). Hence, velocity anomalies in
235 cross sections of slabs that dip in this vertical plane tend to be elongated in a down dip direction and
236 lose amplitude, whereas structures trending perpendicular to this direction tend to be broadened
237 along strike of the slab (Paffrath et al. 2021b, their Fig. 10). Generally, vertical smearing is greater at
238 shallow depths and horizontal smearing increases with depth. Whereas the general recovery of the
239 positions of the coarse checkerboard anomalies (75 x 75 x 60 km) is excellent down to the bottom of
240 the inversion domain at 600 km, the amount of smearing increases with depth, decreasing the
241 resolution below ~400 km to several tens of kilometers.

242 For smaller scale anomalies (50 x 50 x 45 km), recovery of the pattern in checkerboard tests is
243 impeded already below ~300 km depth, where smearing in the NW-SE direction as well as with depth
244 becomes more significant. Also, the amplitude of these smaller anomalies decreases strongly at
245 greater depths. Paffrath et al. (2021b) state that anomalies below the 600 km depth marking the
246 lower boundary of their inversion domain may be amplified and thus appear to lie above this
247 boundary. This is due to the hybrid approach of their tomography ~~that~~ only accounts for three-
248 dimensional velocity perturbations within the inversion domain. To conclude this section, Paffrath et

Deleted: which

250 al. (2021b) show that their source-receiver setup is able to distinguish fundamental differences in the
 251 geometry of slabs on the scale of tens to hundreds of km, thus aiding us in interpreting these
 252 structures.

253
 254
 255 **3. Observations of mantle velocity structure**

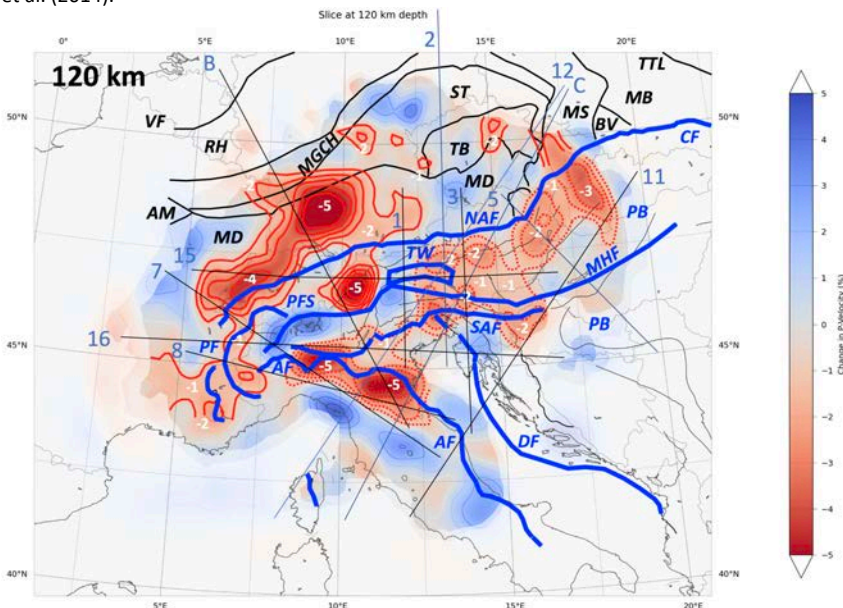
256 For highlighting and interpreting the major mantle structures, we found it useful to trace contours
 257 of both positive and negative velocity anomalies in horizontal tomographic depth slices, then
 258 superpose these traces on the tectonic map of the Alps (Fig. 2) and compare them with anomaly
 259 contours in profiles across the orogen (Figs. 3-6). The surface locations of the aforementioned plate
 260 boundaries on these profiles are used as markers (e.g., Fig. 7). Also included in the profiles is the
 261 trace of the 7.25 km/s iso-velocity contour from the P-wave local earthquake tomography images of
 262 Diehl (2009). We use this contour as a proxy for the Moho in the entire Alps in lieu of other Moho
 263 models which are either local in their coverage (e.g., Behm et al., 2007; Brückl et al., 2007 in the
 264 Eastern Alps) or were found to provide inconsistent estimates of the Moho depth (Spada et al.,
 265 2013, e.g., in the Apennines and Ligurian region). The reader is referred to Kind et al. (2021) for a re-
 266 assessment of Moho depth. The Alpine crustal structure in the profiles is taken from cross sections
 267 of Schmid et al. (2004, 2013, 2017) and Cassano et al. (1986), whereas the pre-Alpine structure in
 268 the Alpine foreland is from Franke et al. (2017), Franke (2020), Mazur et al. (2020) and Schulmann
 269 et al. (2014).

Deleted: M

Deleted: Alpine

Deleted: schematic Variscan crustal cross sections

Deleted: are



270
 271 **Figure 2:** Horizontal V_p tomographic slice at 120 km depth in the mantle. Blue and red areas represent positive
 272 ($+V_p$) and negative ($-V_p$) anomalies, respectively. Contours of slow anomalies emphasized with thick red lines. Solid
 273 red contours - negative velocity anomalies interpreted to correspond to pre-Alpine compositional domains;
 274 dashed red lines - negative velocity anomalies interpreted to correspond to positive thermal anomalies in the
 275 mantle (see text for explanation). Thin black lines indicate the traces of all the profiles displayed in Figures 3 to 6.

280 Thick blue lines – main Alpine structures: NAF - North Alpine Front, SAF – Southern Alpine Front; Other Alpine
281 structures and related features: PFS - Periadriatic Fault System, PF – Penninic Front, TW – Tauern Window, PB –
282 Pannonian Basin, MHF – Mid-Hungarian Fault Zone, WCF – Western Carpathian Front. Thin black lines – Variscan
283 boundaries: VF – Variscan orogenic front, RH – Rheno-Hercynian, MGCH – Mid-German Crystalline High, ST – Saxo-
284 Thuringian, MD – Moldanubian, TB – Tepla-Barrandian, AM – Armorican Massif, BR – Bruno-Vistulian, MB –
285 Malopolska Block, MS – Moravo-Silesian. Other faults: TTL - Teyseyre-Thornquist Line.

286
287 A striking feature in horizontal slices at 100 to 220 km depth is the lateral continuity of $-v_p$
288 anomalies of up to 5-6% which reaches from the northern Alpine foreland across the Alpine
289 orogenic front to beneath the Western and Central Alps, as well as the westernmost part of the
290 Eastern Alps (Fig. 2, solid red contours). In three profiles crossing these parts (profiles B, 1 of Figs.
291 3B, 3C, 4A), $+v_p$ and $-v_p$ anomalies in the 100-220 depth interval form coherent, inclined layers and
292 together outline a package that dips beneath the Alpine front to below the center of the orogen. In
293 the next section, we explain why the base of this package is interpreted to be the base of the
294 downgoing European lithosphere, or lithosphere-asthenosphere boundary, LAB. This layered
295 structure continues down-dip to the SE and beneath the core of the orogen, where it is interrupted
296 (Figs. 3B, 4A). The putative location of the Alpine Tethys suture projected downward into the
297 mantle in all profiles (dashed green line) is hypothetical and drawn in all profiles merely to show the
298 affinity of the former Adria-Europe plate boundary to the European slab (see chapter 5). Profile 8
299 across the foreland of the southernmost Western Alps (Fig. 3A) contains part of the Moldanubian
300 core of the Variscan orogen (Franke et al., 2017) and differs from other profiles across the Alps in
301 featuring only a high velocity layer to some 150 km depth and dipping slightly beneath the front of
302 the Alps.
303

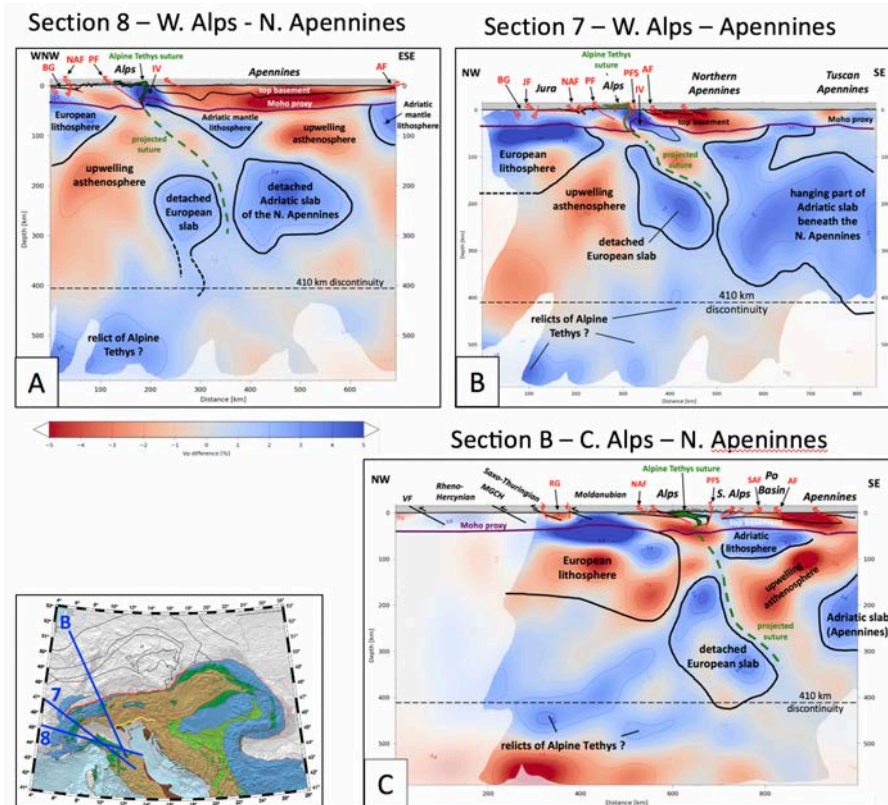
Deleted: The

Deleted: , which corresponds to the base of the moving plate and/or slab in a strictly structural-kinematic sense...

Deleted: e

Deleted: making up the European lithosphere (see next chapter below) ...

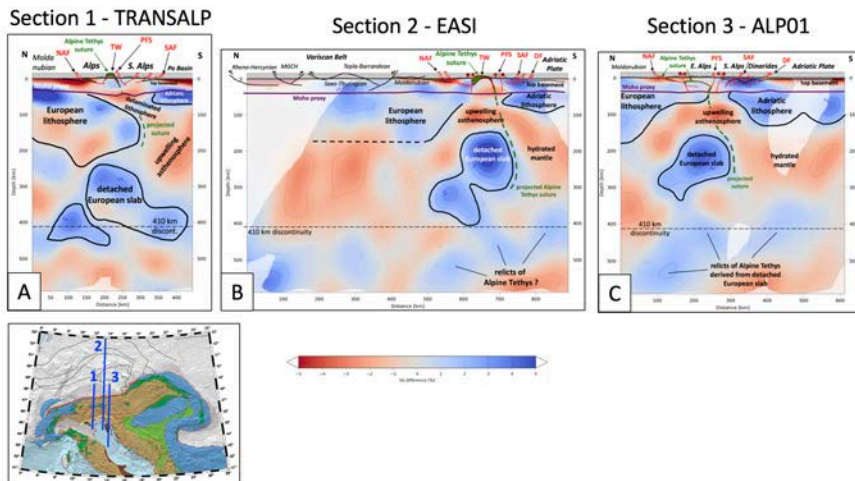
Deleted: , marking a slab tear



311
 312 **Figure 3:** Cross sections of the Western and Central Alps along traces of profiles 8, 7 and B shown in inset: (A)
 313 Western Alps; (B) Western Alps from the Bresse Graben to the Northern Apennines, parallel to profile B of
 314 Lippitsch et al. 2003; (C) Central Alps from the Variscan Belt to the Po Basin and Northern Apennines. Black solid
 315 lines: outlines of the European lithosphere, Adriatic lithosphere and detached to semi-detached slab material.
 316 Green dashed line – putative trace of Alpine Tethys suture based on the location of this suture in the schematic
 317 crustal cross sections depicted above the Moho proxy. The Moho proxy follows the V_p contour of 7.25 sec^{-1}
 318 obtained from the 3D crustal model of Diehl et al. (2009), part of the *a priori* model for obtaining crustal
 319 correction that was incorporated into the tomographic model (Section 2). Geological cross sections largely after
 320 Schmid et al. (2004, 2013, 2017) and Cassano et al. (1986); Variscan crustal cross sections after Franke (2017,
 321 2000), Mazur et al. (2020), and Schulmann et al. (2014).
 322

323 Strong $-v_p$ anomalies of 3-5% (contoured solid red in Fig. 2) generally underlie the central
 324 and western parts of the Moldanubian domain in the Alpine foreland, and run somewhat oblique to
 325 the Variscan domain boundaries. They are not aligned with the Tertiary Bresse and Rhine Grabens
 326 of Oligocene age (Fig. 1). Further to the east, in the area traversed by profiles 2 and 3 (Fig. 2), the
 327 subhorizontally oriented European lithosphere is characterized by dominantly positive velocity
 328 anomalies that cross beneath the front of the Alps and abut a low velocity area in the central part of
 329 the Alps (see Figs. 4B & 4C; stippled red contours in Fig. 2). A large 2% positive anomaly underlies

330 the Moldanubian and Tepla-Barrandean domains beneath the foreland of the Eastern Alps, but does
 331 not extend beneath the orogenic front of the Eastern Alps (Fig. 2; profiles 2 and 3 in Figs. 4B, 4C).
 332



333
 334 **Figure 4:** Cross sections of the Eastern Alps along traces 1, 2 and 3 shown in inset: (A) profile 1 (TRANSALP profile)
 335 from the Variscan foreland to the Po Basin. The thick European lithosphere has the same structure as beneath the
 336 Central Alps (Fig. 3) and is partly detached; (B) Profile 2 (EASI profile) from the Variscan Belt to the Dinaric Front
 337 and Adriatic Plate. The base of the European lithosphere is mostly undefined seismically and the European slab is
 338 detached; (C) Profile 3 (ALP01 profile) from the Variscan Belt to the Adriatic Plate. See legend of Fig. 3 for further
 339 explanations. Alpine and related structures: NAF - North Alpine Front, SAF - Southern Alps Front; PFS - Periadriatic
 340 Fault System, TW - Tauern Window, DF - Dinaric Front

341
 342 In the Eastern Alps, the negative anomaly contours at 120 km depth in Fig. 2 (dashed red
 343 contours) form a broad maximum of 2-5% in map view located between the Northern and Southern
 344 Alpine fronts, and extending eastward from beneath the middle of the Tauern Window to the
 345 Pannonian Basin. Beneath the Eastern Alpine foreland, the upper 80-100 km are characterized by a
 346 broad, moderately positive v_p anomaly of 1-2%. This eastern area shows no horizontal layering of
 347 $+v_p$ and $-v_p$ anomalies (profiles 2 and 3 of Figs. 4B, 4C), in contrast to the layering seen beneath the
 348 foreland in the profile immediately to the west (profile 1, Fig. 4A). The mantle structure beneath the
 349 core of the Eastern Alps (profile 15, Fig. 5A) and beneath the transition to the Pannonian Basin
 350 (profiles 3 and 15, Figs. 4C, 5A) is marked by a shallow, strongly negative anomaly lid and, at depths
 351 between 150 and 400 km, by a strong, blob-like positive anomaly (5-6%) surrounded by a negative
 352 anomaly and unconnected to the Alpine-Carpathian foreland (profiles 2, 3, 12 in Figs. 4B, 4C, 6A).
 353 The pronounced E-W change in anomaly structure below the core of the Alps is best seen in the
 354 orogen-parallel profiles (profile 15, Fig. 5A), where the 150-200 km thick positive-negative velocity
 355 layering characteristic of the Central and Western Alps gives way in the Eastern Alps, more precisely
 356 beneath the western Tauern Window, to a negative anomaly extending down to about 130 km
 357 underlain by the deep (130-300 km) positive anomalies mentioned above. In the next chapter, we
 358 relate this orogen-parallel change to a first-order difference in the structure and composition of the
 359 subducted and delaminated slabs beneath the Alps.

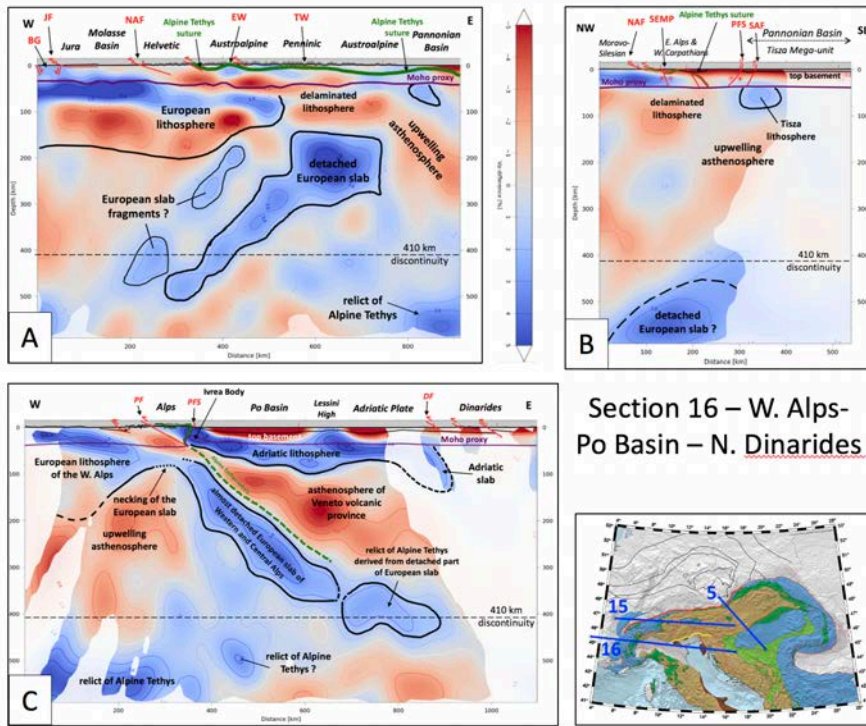
Deleted: de

Deleted: interpret

Deleted: represent

363 The transitional area between Eastern Alps and Western Carpathians (profile 5, Fig. 5B) and
 364 the Pannonian Basin (profile 11, Fig. 6B) is characterized by widespread $-v_p$ anomalies and by the
 365 almost complete absence of $+v_p$ anomalies above the 410 km discontinuity marking the top of the
 366 Mantle Transition Zone. These $-v_p$ anomalies extend to the shallow mantle and directly underlie the
 367 7.25 km/s Moho proxy marking the base of thinned orogenic crust. Weak $+v_p$ anomalies directly
 368 below the Moho are restricted to small parts of the Pannonian Basin (profile 11 in Fig. 6B).
 369 However, stronger $+v_p$ anomalies underlying the Moho are found beneath the Adriatic Sea (profiles
 370 1, 2, 3 and 11, Figs. 4A-C, 6B), marking the still largely undeformed part of the plate of the same
 371 name.
 372

Section 15 – C. Alps – E. Alps – Pannonian B. Section 5 – Pannonian B.

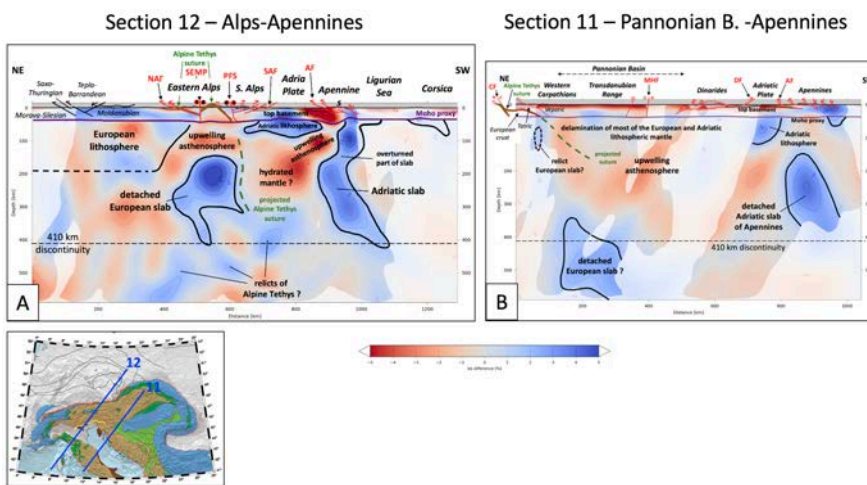


373 **Figure 5:** Cross sections of the Alps along traces 15, 5 and 16 shown in inset: (A) Orogen-parallel profile 15 from
 374 the Central Alps across the Eastern Alps to the Pannonian Basin; note the decrease in thickness of the European
 375 lithosphere before its delamination from the crust at and east of latitude 12°E crossing the area of the western
 376 part of the Tauern Window (TW); (B) Profile 5 from the Variscan Belt in the northwest to the Pannonian Basin in
 377 the southeast across the transitional area between Eastern Alps and Western Carpathians. The European
 378 lithosphere has completely delaminated during Neogene stretching in the greater Pannonian area that formed a
 379 backarc basin in the upper plate consisting of the ALCAPA and Tisza Mega-units during Carpathian rollback
 380 subduction. See legend of Fig. 3 for further explanations; (C) Profile 16 from the Western Alps across the Po Basin
 381 to the northern Dinarides (same as profile M1 in Paffrath et al. 2021b); note the apparent dip of the still-attached
 382

383 European slab beneath the Western and Central Alps, as well as the trace of a slab of Adriatic lithosphere under
384 the northern Dinarides.

385
386 Beneath the northern Dinarides (profile 11, Fig. 6B), no positive anomaly deeper than 100
387 km is observed. However, somewhat further to the north, beneath the northernmost Dinarides in
388 Istria crossed by profile 16 (Fig. 5C), a generally northeast-dipping slab anomaly is fairly well
389 resolved beneath the Dinaric Front, reaching a depth of about 140 km. Note that profile 16 is the
390 same as that presented as profile M1 in Paffrath et al. (2021b).

391



392
393 **Figure 6:** Profiles 12 and 11 along traces shown in Figs. 1 and 2 across the greater Alpine area, Adria and the
394 Apennines: (A) Profile from the Variscan Belt across the Eastern Alps to the northern Apennines and the Ligurian
395 Basin. The European slab beneath the Alps is detached, whereas the Adriatic slab beneath the Apennines hangs
396 subvertically and is partly overturned (see text); (B) Profile from the Central Western Carpathians across
397 Pannonian Basin, northern Dinarides, Adriatic plate, Central Apennines to the Tyrrhenian Sea. The European
398 lithosphere is completely delaminated, the Adriatic slab beneath the Dinarides is almost absent and the Adriatic
399 slab beneath the Apennines is detached from a remnant of the Adriatic lithosphere beneath the Adriatic Sea. See
400 legend of Fig. 3 for further explanations. Alpine faults and related structures (labeled red): NAF - North Alpine
401 Front, SAF - Southern Alps Front, PFS - Periadriatic Fault System, SEMP - Salzach-Ennstal-Mariazell-Puch Fault,
402 MHF - Mid-Hungarian Fault Zone, CF - Carpathian Front, DF - Dinaric Front, AF - Apennine Front.

403
404 A large, subvertically dipping positive anomaly directly below the Northern Apennines in profile
405 12 (Fig. 6A) is only connected to the crust near the Ligurian Sea and disconnected from the flat-lying
406 high V_p mantle below the undeformed part of the Adriatic Plate further to the NE. This Adria-
407 derived slab dips down to the 410 km discontinuity. Further to the southeast beneath the Tuscan
408 Apennines in profile 11 (Fig. 6B), this anomaly is completely disconnected from the orogenic crust
409 and dips steeply to the SW in a depth interval of 100-350 km. In a profile parallel to the Apennines
410 (profile 7, Fig. 3B), this positive anomaly is seen to lose its connection with the orogenic crust
411 between profiles 12 and 11 in Figs. 6A and 6B. Unfortunately, the resolution drops off to the SW
412 beneath the Ligurian and Tyrrhenian Seas, but the faint anomalies in the former region suggest that
413 the Moho proxy is directly underlain by a negative anomaly.

414

Deleted: The resolution is poor in this area, but the interpretation is in line with previous teleseismic studies (e.g., Bijwaard & Spakmann, 2000; Wortel & Spakmann, 2000; Piromallo and Morelli, 2003; Spakman and Wortel, 2004; Serretti and Morelli, 2011; Koulakov et al., 2009). ...

Deleted: de

Deleted: f

422 **4. Choices in the interpretation of seismic structure**

423 The tomographic profiles in Figs. 3-6 depict relative velocities as percentages of deviation from a
424 mean velocity model for crust and mantle (Paffrath et al. 2021b). There are two main challenges in
425 interpreting the anomaly patterns down to a depth of around 600 km: (1) Distinguishing the effects
426 of the present thermal state of the rocks from composition and structural anisotropy on the
427 anomalies. This is difficult, if not impossible, in the absence of corroborative evidence from
428 independent approaches, e.g., heat flow, gravity, conductivity and/or other seismological methods;
429 (2) accounting for poor resolution of the tomographic images that often precludes a unique
430 determination of the geometry of the anomalies. This is especially true of anomalies at great depth
431 in the mantle, where vertical smearing blurs the images (Foulger et al., 2013).

432 Further headway in interpretation can be made by invoking geological criteria and what we
433 broadly call “the geodynamic context” in order to weigh the consistency, and therefore the
434 plausibility, of some interpretations over others. To illustrate this important point, we consider
435 profile B across the Central Alps in Fig. 3C, shown without interpretation in Fig. 7A and with two
436 contrasting interpretations in Figs. 7B and 7C. This profile is a good place to begin our interpretative
437 foray, because the geology (i.e., structure, kinematics, metamorphism, thermal and stratigraphic
438 ages) is well known along this classic section of the Alps (e.g., Schmid et al., 1996, 2004) and
439 previous active-source seismology provides tight constraints on the crustal structure down to the
440 Moho (Pfiffner and Hitz, 1997) and other sources in NFP-20 volume (Pfiffner et al. 1997, eds).

441 The uninterpreted profile B of Fig. 7A shows two main features:(1) the positive-negative
442 anomaly layering extending down to about 200 km observed in the Alpine foreland and extending
443 to well south of the Northern Alpine Front down to 180 km depth, as described in the previous
444 section; and (2) domains of deep-seated positive anomalies labeled with question marks, one
445 dipping northward from the Southern Alps down to the 410 km discontinuity below the Alpine
446 foreland, a second minor one dipping southward below the Po Basin. In Fig. 7B, the positive-
447 negative anomaly layering is interpreted to make up a coherent kinematic entity that moved as a
448 unit with respect to the orogenic front and was subducted to the SSE beneath the Adriatic Plate in
449 Tertiary time. A post-subduction age of this layering can be ruled out in the absence of a post
450 Tertiary thermal event corresponding to the lateral extent of the $-V_p$ anomaly in Figure 2. The $-V_p$ is
451 therefore interpreted in Figure 7B to form the bottom half of the lithosphere, i.e., the non-
452 convecting part of the mantle.

453 We point out that not all plates in the greater Alps area comprise such thick, heterogeneous
454 lithosphere. Indeed, as shown in the next section, the Adriatic Plate and the Adria-derived slab
455 beneath the Apennines comprise lithosphere in the standard sense of a seismically “fast”, more
456 homogeneous kinematic entity.

457 The slab of thick lithosphere descending beneath the Northern Alpine Front in Fig. 7B is
458 interpreted to be broken, with its fragment continuing down to the 410 km discontinuity beneath
459 the Po Basin. Weaker positive anomalies beneath the Alps in the 300-600 km depth interval may be
460 subducted and detached relicts of the Alpine Tethyan Ocean. However, resolution is poor at these
461 depths, so our interpretation of such relicts is speculative, as signified by question marks in the
462 figures.

463 In the interpreted profile B (Fig. 7B) other $-V_p$ anomalies in the mantle occur immediately
464 beneath the Moho in the cores of the Alps and Apennines where the Moho lies at c. 50 km depth
465 and where the lower crust is also characterized by low V_p . Finally, a deep-seated $-V_p$ anomaly is
466 found below the Adriatic lithosphere, between the detached part of the European slab and the
467 Northern Apennines slab derived from Adriatic lithosphere (Fig. 7B). In the former case, the $-V_p$
468 anomaly in the mantle immediately below the Moho is interpreted to manifest a depression of the

Deleted: ¶

Deleted: s

Deleted: south

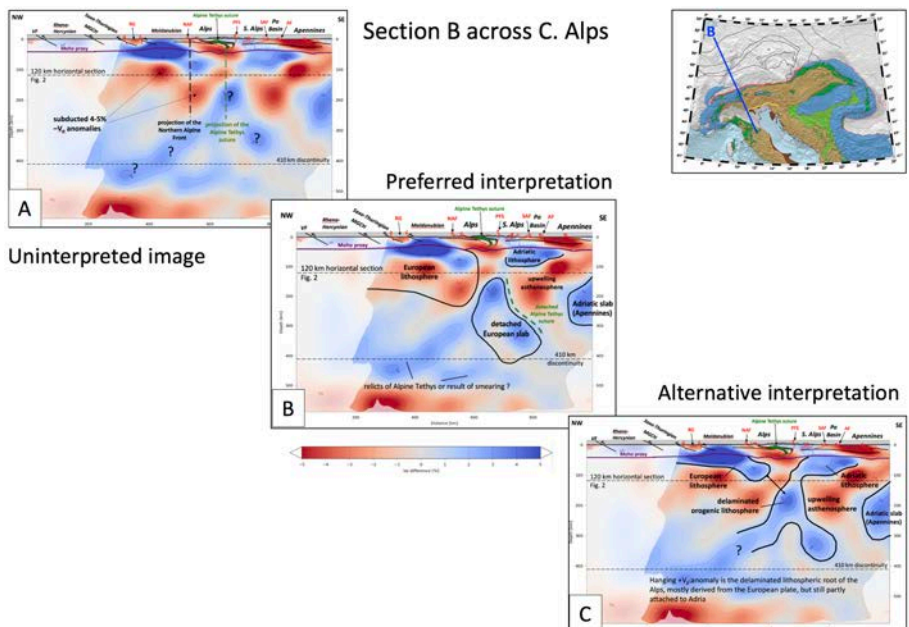
Deleted: .

Deleted: layer

Deleted:

Deleted: f

476 absolute velocities by the occurrence of hydrous, less-dense and therefore seismically slower
 477 material in the subduction channel. In the case of the deep-seated $-V_p$ anomaly labeled “upwelling
 478 asthenosphere”, the negative anomalies of up 5-6% could possibly be caused by still hot, upwelling
 479 asthenosphere. However, as argued in section 6.3, this would need a ΔT of some 600-700°C
 480 resulting in temperatures well above 1400°C. Following the suggestion by Giacomuzzi et al. (2011),
 481 we envisage hydrated, possibly decarbonated mantle (Malusà et al. 2018, 2021) in a backarc
 482 position behind the descending non-detached and detached parts of the European lithosphere
 483 rather than still-existing, substantially elevated temperatures as a suitable explanation for the low
 484 V_p in this area.
 485



486 **Figure 7:** Raw image of vertical tomographic profile B across the Central Alps and two alternative interpretations:
 487 (A) Raw image showing layered positive and negative V_p anomalies extending from the Variscan Belt to south of
 488 the Northern Alpine Front (NAF, see also Fig. 2); (B) Preferred interpretation shown in Fig. 3C, indicating
 489 coherence of layered positive and negative V_p anomalies that are interpreted as thick and old (Variscan or older?)
 490 European lithosphere dipping to the south beneath the Alps. The European slab is detached. In contrast, the
 491 Adriatic lithosphere beneath the Po Basin and Apennines is thin and underlain by a large negative anomaly
 492 interpreted as upwelling asthenosphere; (C) Standard interpretation of lithosphere as comprising only positive V_p
 493 anomalies, thought to be old, cold lithosphere. The long N-dipping positive V_p anomaly is interpreted as the
 494 delaminated lithospheric root of the Alps, mostly derived from the European Plate, but still partly attached to the
 495 Adriatic Plate (see text for discussion).
 496
 497

498 In the contrasting interpretation shown in Fig. 7C, all anomalies are considered primarily to
 499 reflect temperature anomalies, such that positive anomalies at depths below the Moho are
 500 interpreted as subducted lithosphere, whereas negative anomalies below the Moho are equated
 501 with hot asthenosphere and are not part of a subducted plate. This is in line with the thermo-

502 rheological definition of a descending sheet of rigid and cold lithosphere. Thus, the base of the
503 positive anomaly extending from the European foreland to below the Northern Alpine Front would
504 mark a descending lithospheric plate only 80 km thick, whereas the long north-dipping, positive
505 anomaly domain in this profile could be interpreted as subducted Adriatic lithosphere connected to
506 Adriatic lithosphere beneath the Po Basin and the Adriatic Sea (Fig. 7C). If true, this would imply a
507 thin European continental lithosphere and necessitate hundreds of kilometers of shortening in the
508 Alps within predominantly S-facing folds and thrusts for which there is no geological evidence. Most
509 folding and thrusting in the Alps is N- to NW-vergent, as documented by more than a century of
510 detailed study. Within the Southern Alps where S-vergent thrusting is indeed observed, only about \leq
511 72 km of shortening was accommodated, mostly in Oligo-Miocene time (Schönborn, 1992; Schmid
512 et al., 1996; Rosenberg and Kissling, 2013). This effectively precludes any scenario involving north-
513 directed subduction of large amounts of Adriatic lithosphere beneath the Alps. Moreover, the
514 continuity of the NW-dipping +Vp anomaly in Fig. 7C may reflect smearing, which is prevalent in
515 profiles with this azimuthal orientation (see section 2 above).

516 This leaves Fig. 7B with its anomalously thick (180-200 km) subducting European lithosphere as
517 the preferred interpretation. The total length of subducted European slab according to the
518 interpretation in Fig. 7B is roughly 400 km, as measured between the Northern Alpine Front down
519 to the 410 km discontinuity (see also profile 6 in Appendix A1). This is consistent with the amount of
520 shortening in the Alps since European lithosphere entered the subduction zone in the Alps in
521 Eocene time (Schmid et al., 1997; Handy et al., 2010), lending further support to our interpretation.
522 We return to this point in section 6 below.

523
524

5. Regional tectonic interpretation

525 In interpreting the images in Figs. 3-6 and all the additional profiles in Appendix A, we marked
526 boundaries (thick black lines) around kinematically coherent images whose geometry is consistent
527 with available data on Moho depth and with the kinematic history of tectonic units exposed at the
528 surface. Dashed solid black lines delimit very poorly defined or even putative boundaries. The base
529 of the European foreland lithosphere in the Central Alps is well defined and taken to be the base of
530 the -Vp layer at about 180 km depth, as discussed in the previous section (profiles 1, 4, 6, 9, 15 and B
531 in Appendix A). In other profiles, especially in the Eastern Alps where the base of the lithosphere is
532 poorly defined, we placed the lower boundary at approximately the same 180-200 km depth to
533 avoid abrupt along-strike variations in lithospheric thickness beneath foreland crust with the same
534 Variscan and pre-Variscan history. Thus, some boundaries are drawn across seismically fast and
535 slow domains, highlighting the difficulty of using solely seismological criteria to define the LAB
536 (Artemieva, 2011). In Figs. 8 and 9, we include two horizontal depth slices at 240 km and 90 km,
537 respectively, to show the main structures outlined by velocity anomalies in map view.

538
539

5.1 Alps

540 European lithosphere of Variscan and/or pre-Variscan origin originating in the Alpine foreland is
541 evident in all cross sections of the Central Alps (Figs. 3, 4), though its base in the Eastern Alps is
542 undefined (e.g., profile 2 in Fig. 4B). Beneath the Central Alps and westernmost Eastern Alps, this
543 lithosphere dips to the S to become the thick, subducted European slab (profiles B and 1 in Figs. 3C,
544 4A), whereas in the Western Alps (profiles 8 and 7 in Figs. 3A, B) and in the Eastern Alps east of 12°E
545 (profiles 2, 3 and 12 in Figs. 4B, C, 6A), the European slab is completely detached from its foreland.
546 Only in the transitional area between Western and Central Alps is the slab still tenuously connected
547 to the European lithosphere of the Alpine foreland (profile 16, Fig. 5C). The moderate dip and
548

Deleted: f

Deleted: n

Deleted: anomalously

Deleted:

553 inordinate length of the slab beneath the entire E-W extent of the Po Basin in this particular profile
554 reflect the fact that this W-E running profile obliquely slices the European slab at a high angle to the
555 SE dip of Alpine subduction in the Western and Central Alps. Moreover, the E-dipping positive
556 anomaly seen in Fig. 5C comprises different pieces, with the positive anomaly at the eastern end
557 (below the Adriatic plate east of the Lessini Mountains, at a depth of around 350-450 km)
558 originating from a south-dipping slab fragment below the Eastern Alps depicted in Fig. 4A. This
559 easternmost part of the positive anomaly in profile 16 of Fig. 5C also slices minor, discontinuous
560 relics of Alpine Tethys south of the main slab in the Eastern Alps (see lower right-hand side of N-S
561 trending profile 2 in Fig. 4B).

562 In the Western Alps, detachment of the European slab (Figs. 3A, 3B) was previously noted by
563 Lippitsch et al. (2003) and interpreted as a subhorizontal tear that is currently propagating from SW
564 to NE towards the still-attached part of the slab in the western Central Alps (Kissling et al., 2006).
565 The detachment of this part of the slab (profile A in Appendix A), possibly combined with unloading
566 due to glacial erosion and melting (Champagnac et al., 2007; Mey et al., 2016), have been deemed
567 responsible for rapid Plio-Pleistocene exhumation and surface uplift of the Western Alps (Fox et al.,
568 2015, 2016) which have the highest peaks (up to 5000 m) and greatest relief (3000 m) of the entire
569 Alpine chain.

570 In the Eastern Alps, the detached European slab hangs subvertically to steeply N-dipping in a
571 depth interval ranging from 150 to 350-400 km. We note that the pronounced along-strike change
572 in orogenic mantle structure between nearby profiles 1 and 2 (Figs. 4A and 4B) does not coincide
573 with the Austroalpine-Penninic boundary marking the Alpine Tethys suture between the Central and
574 Eastern Alps at the surface. This along-strike change is best seen by comparing the mantle structure
575 in an orogen-parallel profile with the location of the suture in the tectonic map (profile 15 in Fig. 5A)
576 and its projected trace in the horizontal depth slice at a depth of 90 km (Fig. 9). Rather, it coincides
577 with the northward projection of the Giudicarie Belt (marked GB in Fig. 1), a post-collisional fault of
578 latest Oligocene to Miocene age (Pomella et al., 2012) which sinistrally offsets the eastern and
579 southern parts of the Alpine orogenic edifice, including the Periadriatic Fault System (Verwater et
580 al., 2021). The northward projection of the Giudicarie Belt, which lies in the Tauern Window in map
581 view, coincides with the westernmost point of eastward, orogen-parallel extrusion of the Alpine and
582 Western Carpathian lithosphere in latest Oligocene to Miocene time (e.g. Scharf et al., 2013; Schmid
583 et al., 2013; Favaro et al., 2017). This allochthonous block is referred to in the literature as the
584 ALCAPA mega-unit. The orogenic Moho beneath this block shallows dramatically to the east (e.g.,
585 Grad et al., 2009; Kind et al., 2021), reaching a depth of some 20 km beneath the Pannonian Basin
586 (profiles 15 and 5 in Figs. 5A, B). The occurrence of negative V_p anomalies and reduced gravity
587 anomalies (Zahorec et al., 2021) immediately below this shallow orogenic Moho in the Eastern Alps
588 (e.g., profile 12, Fig. 6A, highlighted low V_p area in Fig. 9) strongly suggests that the entire
589 lithospheric mantle reaching from the Tauern Window of the Eastern Alps to their transition with
590 the western Carpathians (profile 5 in Fig. 5B) has been delaminated.

592 5.2 Pannonian Basin

593 The negative V_p anomaly of the Eastern Alps continues further to the NE to beneath the Vienna
594 Basin and the Central Western Carpathians, as seen in the 90 km and 120 km depth slices (Figs. 2,
595 8). This is the area overlying slab remnants that have descended into the Mantle Transition Zone
596 (e.g., profile 5 in Fig. 5B). The Central Carpathians host a province of 17-14 Ma post-collisional sub-
597 alkaline magmatism (Seghedi and Downes, 2011; Seghedi et al., 2013) related to Miocene extension
598 of the Pannonian domain ~~in the upper plate of the Western Carpathian orogen~~. Given the fact that
599 this magmatism ended some 14 Ma ago, it is uncertain if the low V_p anomaly in the Western

Deleted: ,

Deleted: including the

Deleted: s

603 Carpathians is solely related to a persistent positive thermal anomaly. In this context, it is relevant
604 to note that the area of the Tisza mega-unit south of the Mid-Hungarian Shear Zone (MHZ in Fig. 1)
605 and characterized by high heat flux (Horvath et al., 2015, their Fig. 12) does not exhibit such a
606 negative V_p anomaly. This indicates that present-day heat production does not everywhere
607 correlate with negative seismological anomalies.

608 Relicts of delaminated and detached European lithosphere can be detected at and below the
609 410 discontinuity beneath the Pannonian Basin (profiles 5 and 11 in Figs. 5B, 6B) as previously
610 discovered in the passive array swath experiment of Dando et al. (2011). As mentioned in discussing
611 Fig. 7, the 400 km down-dip length of the slab segments is broadly consistent with estimates of
612 shortening since the European slab entered the subduction zone after the closure of Alpine Tethys
613 at around 40 Ma (e.g., Schmid et al., 1996; Handy et al., 2010; Kurz et al., 2008). This suggests that
614 the detached slab remnants comprise mostly European lithosphere (Mitterbauer et al., 2011;
615 Rosenberg et al., 2018; Kästle et al., 2020).

616 5.3 Adriatic Plate

617 The Adriatic Plate is 100-120 km thick as defined by the lower limit of the horizontal $+V_p$ anomalies
618 beneath the Adriatic Sea. We label this as Adriatic lithosphere and regard it as Adriatic lithosphere
619 in a kinematic sense (e.g., profiles 1, 2, 3 and 12 in Figs. 4, 6A). This is less than half the thickness of
620 the European lithosphere. It is generally accepted that in the Alps the former Adriatic Plate formed
621 the upper plate during convergence, whereas in the Dinarides and Apennines, Adria is the
622 subducting plate. The Adriatic slab in the Apennines possibly has a simpler velocity structure than
623 the European slab in the Alps, comprising thinner and compositionally more homogeneous
624 lithosphere with only $+V_p$ anomalies (Fig. 6). In contrast to the European foreland (Franke, 2020),
625 most of the former Adriatic Plate was not affected by high-grade metamorphism and never
626 experienced the closure of various Paleozoic oceans. Instead, it has been interpreted as the
627 southern, Gondwana-derived foreland of the Variscan belt (Molli et al., 2020).

628 The Adriatic lithosphere is underlain by a pronounced low-velocity mantle in depth interval
629 of 150-350 km (profiles B and 3 in Figs. 3C, 4C right hand side; profile 12 in Fig. 6; profiles B, 3, 12,
630 11 in Appendix A). This thick low-velocity zone coincides at the surface in the eastern Po Basin and
631 northern Adriatic Sea with the Veneto volcanic province (Figs. 1, 8), which comprises mostly
632 primitive basalts diluted by a depleted asthenospheric mantle component (Macera et al., 2003). Its
633 age range between Late Paleocene to Late Oligocene (Beccaliva et al., 2007) spans the transitional
634 time from subduction to collision in the Alps (Handy et al., 2010 and refs therein). It is thus tempting
635 to attribute this magmatism to the combined effects of heat and fluid advection behind the
636 originally S-dipping European slab in the Alps (Macera et al., 2008). The release of water and
637 incompatible elements from deeply buried sediments along the slab interface may have caused
638 hydration of the overlying mantle, giving rise to an overall decrease in seismic velocity, as proposed
639 by Giacomuzzi et al. (2011) to explain the negative anomaly layer beneath the Adriatic Plate.

641 5.4 Apennines

642 Switches in the polarity of subduction are manifested at the surface by changes in thrust vergence
643 and location of the orogenic fronts at the Alps-Apennines and Alps-Dinarides junctions (Fig. 1). The
644 mantle structure at the Alps-Apennines junction is simpler than the complex surface fault structure
645 due to switching subduction polarity (Molli et al., 2010; Schmid et al., 2017) would suggest. There,
646 the European and Adriatic slabs are easily distinguished in profiles 8 and 7 (Fig. 3A, B). In the
647 horizontal slice at 240 km depth in Fig. 8, the two slabs cannot be distinguished at the resolution of
648 the horizontal depth slice because they are very close to each other (see Figs. 3A, B). However, the
649

Deleted: u

Deleted: transitions

Deleted: transition

653 horizontal slice at 90 km (Fig. 9) shows them separated by the downward projection of the Alpine
654 Tethys suture. Note that the European slab beneath the Western and Central Alps was subducted to
655 the SE below the Adriatic Plate prior to 35 Ma, ultimately leading to the Alpine Tethys suture
656 depicted in Fig. 9. Adria-Europe suturing occurred before the Apennines formed in latest Oligocene
657 to Miocene and Pliocene time. When considering profiles 8 and 7 in Fig. 3A, as well as profiles 12
658 and 11 in Figs. 6A and 6B in the following discussion, it is important to note that the Adriatic slab
659 beneath the northern Apennines originally dipped to the SW when it was still attached to the then-
660 still undeformed western part of the Adriatic Plate (Facenna et al. 2004, Schmid et al. 2017).
661 Apenninic orogenesis involved E-directed rollback of this former Adriatic Plate that currently makes
662 up the slab below the Northern Apennines.

663 In profile 12 (Fig. 6A) across the northern Apennines, the upper 200 km of the Adriatic slab
664 anomaly dip to the NE and are hence overturned, as pointed out in section 3. This slab is detached
665 from the Adriatic lithosphere and located in the NE foreland of the Apennines. Somewhat more to
666 the south in profile 11 (Fig. 6B) across the central (Tuscan) Apennines, the Adriatic slab is normally
667 inclined, i.e., dips to the SW, and completely detached from the orogenic wedge of the Apennines.
668 In profile 7 (Fig. 3B) running parallel to the strike of the Apennines slab, a subhorizontal tear is
669 clearly visible beneath the Tuscan Apennines at a depth of 80-100 km. We speculate that once the
670 Apennines stopped advancing in Plio-Pleistocene time (e.g., Molli et al., 2010), the heavy Northern
671 Apennines slab steepened. The subhorizontal tear visible in Fig. 3B appears to have propagated
672 from SE to NW, i.e., in a direction of decreasing orogen-normal shortening in the Apennines and
673 towards the pole for Neogene counterclockwise rotation of the Corsica-Sardinia block with respect
674 to Europe (Speranza et al., 2002), also affecting the Apenninic orogen (Maffione et al., 2008). Partial
675 tearing allowed the detached part of the slab in the SE to retreat and sink under its own weight,
676 while the smaller, still-partly attached segment in the NW became vertical and locally overturned
677 (profile 12 in Fig. 6A). The maximum depth (8-9 km) of Plio-Pleistocene fill in the northern Apenninic
678 foreland or "Po" Basin (Bigi et al., 1989) and the deepest Moho beneath the northern Apennines
679 (50-60 km, Spada et al., 2013) are both attributed to the downward pull of this still partially
680 attached slab segment depicted in profile 12 of Fig. 6A (Picotti and Pazzaglia, 2008).

681 The horizontal depth slice at 90 km in Fig. 9 shows the area traversed by profiles 12 and 11
682 discussed above that is characterized by low V_p and interpreted to outline lithospheric delamination
683 during slab detachment. These areas extend from NW to SE along the front of the NE-facing
684 Apennines nappe stack. This indicates that the Adriatic slab below the Apennines has detached
685 from the little-deformed Adriatic Plate in the Adriatic Sea almost all along the strike of the Northern
686 and Central Apennines. Note that this area of delamination is slightly NE of the outline of the
687 detached and subvertical Adriatic slab shown in the horizontal depth slice at 240 km depth (Fig. 8).
688

689 5.5 Dinarides

690 Our data only cover the area of the northern Dinarides and the Dinarides-Alps junction in Slovenia
691 (Stipčević et al., 2011, 2020). Collisional shortening after the closure of the Neotethyan oceanic tract
692 in the northern Dinarides started earlier than in the Alps; major collisional shortening lasted from
693 Late Cretaceous to Oligocene time, with only very minor shortening in the Miocene (e.g., Schmid et
694 al., 2008). In the Alps, collisional shortening after the closure of Alpine Tethys started later, namely
695 in the late Eocene and lasted until Pliocene times. The junction between the Alps and the Dinarides
696 is marked at the surface by the Southern Alpine Front that thrustured the Southern Alps southward
697 over older NW-SE striking Dinaric thrusts (Fig. 1) in the late Miocene. South-directed thrusting in
698 this transition~~al~~ area, combined with dextral strike slip reactivating Dinaric structures, is still

Deleted: ¶

Deleted: transition

Deleted: area

Deleted: transition

703 seismically active (e.g., Kastelic et al., 2008; see yellow line marking the presently active plate
 704 boundary in the Alps in Fig. 1).

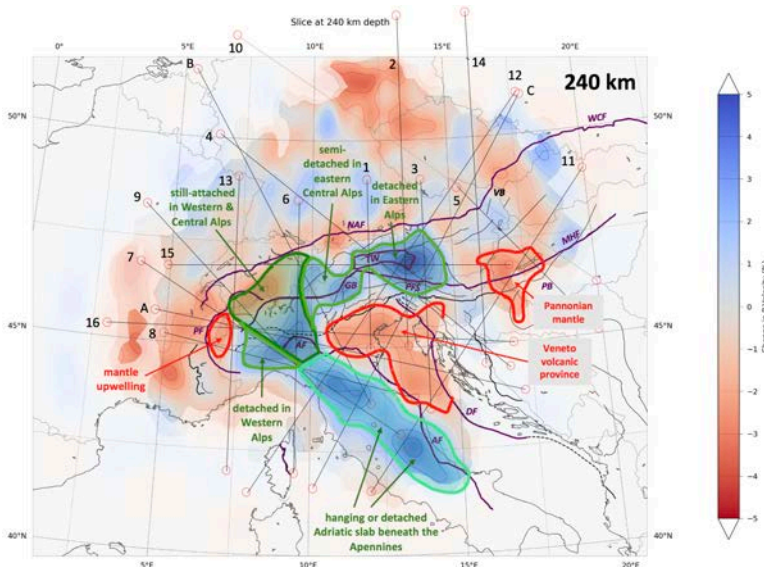
705 An east- to northeast-dipping positive V_p anomaly is partly imaged beneath the Dinarides in
 706 profile 16 (Fig. 5C), but is lacking in profile 11 (Fig. 6B), which crosses the Dinaric Front to the south.
 707 Though the resolution in this latter profile is very poor, the lack of a discernable slab is consistent
 708 with previous teleseismic studies (e.g., Bijwaard & Spakmann, 2000; Wortel & Spakmann, 2000;
 709 Piromallo and Morelli, 2003; Spakman and Wortel, 2004; Serretti and Morelli, 2011; Koulakov et al.,
 710 2009), which support the idea of a slab gap in the northernmost Dinarides. Ustaszewski et al.
 711 (2008), Schefer et al. (2011) and Horvath et al. (2015) invoked asthenospheric upwelling at the SE
 712 limit of the Pannonian basin associated with the breakoff of part of the NE-dipping Adriatic slab.
 713 This is thought to have permitted asthenosphere to flow from beneath the Adriatic Plate to below
 714 the extending Pannonian Basin in the upper plate of the retreating Carpathian subduction (Jolivet et
 715 al., 2009; Handy et al., 2015; Horvath et al., 2015; Kiraly et al., 2018).

716
 717 **5.6 Summary of the tectonic interpretation**

718 We summarize by combining all the profiles in Appendix A as a basis for interpreting horizontal
 719 depth slices (Figs. 8, 9). The 240 km depth slice in Fig. 8 maximizes the number of slabs intersected
 720 and exhibits various degrees of attachment of the slabs to their orogenic edifice and their forelands.
 721 The horizontal depth slice of Fig. 9 at 90 km visualizes areas of negative V_p in the uppermost mantle.
 722

- Deleted: frontal
- Deleted: des
- Deleted: Unfortunately,
- Deleted: .
- Deleted: A
- Deleted: has been recorded by global tomography (Bijwaard and Spakman, 2000; Piromallo and Morelli, 2003...
- Deleted:), possibly due to the previous inability of imaging a slab of only ≤ 140 km length in this area. ...

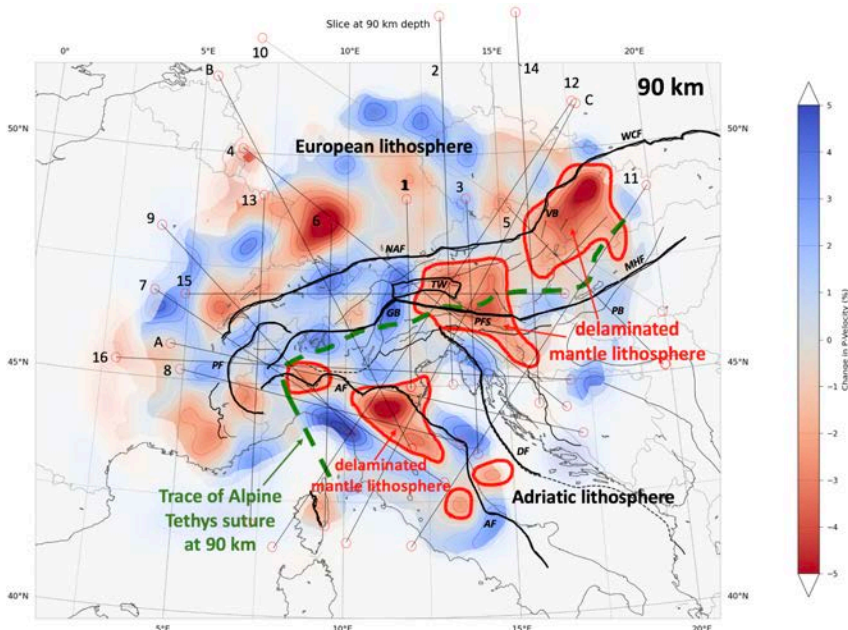
- Deleted: the interpretation of



723 **Figure 8:** Horizontal V_p tomographic slice at 240 km. Blue and red areas represent fast and slow teleseismic p-
 724 wave anomalies, respectively. Isolines indicate deviation in % of P-wave velocities from the mantle model in
 725 Paffrath et al. (2021b). Green lines are boundaries of slabs at their intersection with the horizontal plane of the
 726 depth slice. The slab boundaries were obtained by projecting the interpreted slab outlines marked with black lines
 727 in the 19 profiles in Appendix A (traces shown as thin black lines) into the plane of the depth slice. Shades of green
 728 denote various degrees of attachment of the European slab to the European lithosphere in the Alpine foreland
 729 (see interpreted profiles and text). Red lines outline domains of mantle upwelling. Thick black lines are major
 730

741 Alpine faults: NAF - North Alpine Front, PFS - Periadriatic Fault System, GB – Giudicarie Belt, PF – Penninic Front,
 742 TW – Tauern Window, VB – Vienna Basin, PB – Pannonian Basin, MHF – Mid-Hungarian Fault Zone, AF – Apennines
 743 Front, DF – Dinaric Front.
 744
 745

Deleted: des



746 **Figure 9:** Horizontal V_p tomographic slice at 90 km depth. Blue and red areas represent fast and slow teleseismic
 747 p-wave anomalies, respectively. Isolines indicate deviation in % of P-wave velocities from the mantle model in
 748 Paffrath et al. (2021b). Thick dashed green line is the projection of the suture zone of Alpine Tethys down to 90
 749 km based on interpretation of the profiles. This green line marks the southern boundary of the European Plate
 750 with the Adriatic Plate and the lithosphere of the Tisza megaunit beneath the Pannonian Basin. Note the variable
 751 P-wave velocities within the European lithosphere at this depth due to pre-Alpine tectogenesis. Areas outlined in
 752 red indicate areas with low V_p located within the Alpine-age orogens where shallow asthenosphere replaced
 753 delaminated mantle lithosphere after slab detachment in the Alps, Western Carpathians and the Apennines
 754 occurred.
 755

756
 757 Figure 8 shows that in the Alps, slab attachment is only complete in the Central and northern
 758 Western Alps between 7° and 10°E. This is corroborated by surface-wave tomography (Kaestle et al.
 759 2018, their Fig. 12) indicating continuous positive velocity anomalies down to depths below 180 km
 760 in the Central Alps. Detachment is complete in the southernmost Western Alps and modest in the
 761 eastern Central Alps between 10° and 12°. It is complete in the Eastern Alps east of about 12°E
 762 where we observe the detached Eastern Alps slab (Fig. 8) dipping to the NE (e.g., Lippitsch et al.,
 763 2003; see Figs. 4B, 4C and 6A). No significant positive V_p anomaly is seen at 240 km depth in the
 764 easternmost Eastern Alps and the Western Carpathians east of 15°E, where the relicts of former
 765 slabs reside below the 410 km discontinuity (see Fig. 5). Where detachment is complete, the slabs
 766 have been supplanted by upwelling asthenosphere, as is seen by three areas of negative V_p

768 anomalies outlined in the depth slice for 90 km (Fig. 9) in the southern Western Alps, the Veneto
769 volcanic province and the Pannonian basin. In the Apennines, the Adriatic slab is locally hanging, but
770 mostly completely detached from its overlying orogenic root and foreland. There too, upwelling
771 asthenosphere has locally replaced the descending slab in the frontal, i.e., NE parts of the orogen,
772 eliminating the former connection of the slab with the remaining undeformed part of the Adriatic
773 Plate in the Adriatic Sea.

774 Figure 9 also features a dashed green line marking the location of the Alpine Tethys suture zone
775 projected from the crustal down to 90 km, separating the European lithosphere from the Adriatic
776 lithosphere. We emphasize that the downward projection of this suture in the profiles (dashed
777 green lines) is hypothetical in the sense that mapping it involved tracing the suture through
778 domains that were extensively modified during delamination and mantle upwelling. The severe
779 bending of the putative trace of this suture zone at the Alps-Apennines junction reflects
780 counterclockwise rotation of the Corsica-Sardinia block and the Ligurian Alps in Miocene time
781 (Schmid et al., 2017 and references therein). Likewise, bending of the projected suture north of the
782 Mid-Hungarian fault zone is due to the counterclockwise rotation of the Western Carpathians, also
783 in Neogene time (Márton et al., 2015).

784

785

786 6. Discussion

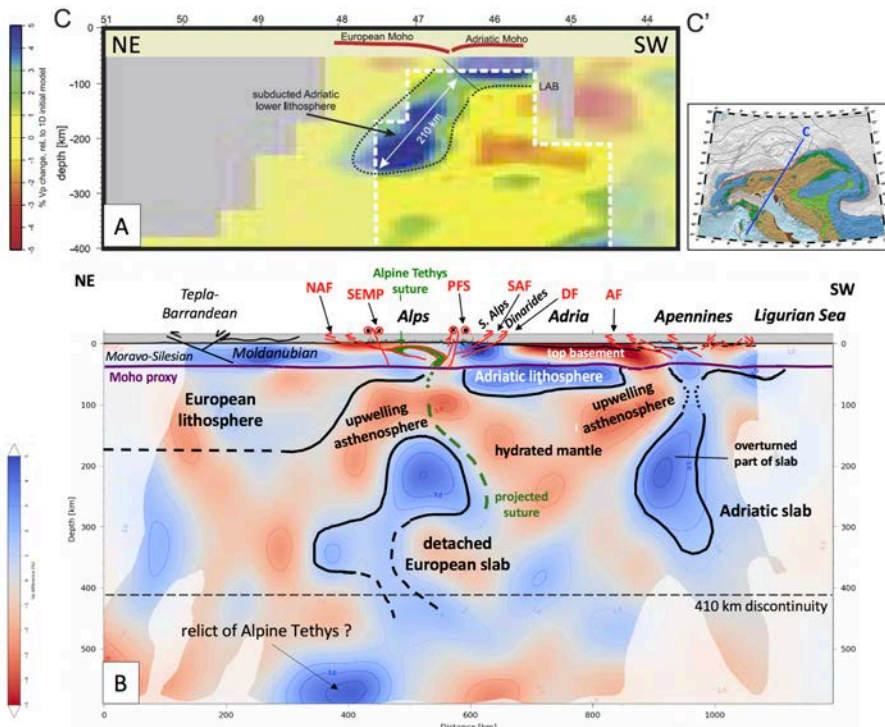
787

788 6.1 Subduction polarity – was there a switch in the Alps?

789 The polarity of subduction in the Alps, particularly at its junction with the northern Dinarides, has
790 been a bone of contention ever since the publication of P-wave tomographic images showing high
791 velocity anomaly some 200 km long dipping some 50° to the NE beneath the Eastern Alps (Babuska
792 et al. 1990) and connected with the upper mantle of the undeformed Adriatic Plate according to
793 Lippitsch et al. (2003). The Eastern Alps slab was thought to be separated from the SE-dipping
794 European slab anomaly in the Central and Western Alps by a decrease in strength of the positive
795 anomaly, interpreted by these authors as a slab gap in map view. The attribution of the Eastern Alps
796 slab to the Adriatic Plate by Lippitsch et al. (2003) was challenged by Mitterbauer et al. (2011),
797 whose teleseismic model showed a steeper (75° or more) and longer Eastern Alps slab reaching
798 down to the 410 km discontinuity. The Eastern Alps slab was thought to have been Adriatic
799 lithosphere that had been laterally wedged from the Dinarides (Lippitsch et al., 2003) or subducted
800 beneath the Eastern Alps in Neogene time (Schmid et al., 2004; Kissling et al., 2006; Handy et al.,
801 2015). Although N-directed subduction was inconsistent with north-vergent nappe stacking along
802 strike of the entire Alpine chain, these authors postulated a late-stage switch in subduction polarity
803 in Miocene times, i.e., after nappe stacking. Another possible problem with a Miocene switch in
804 subduction polarity is that the easternmost part of the slab anomaly imaged by Lippitsch et al.
805 (2003) is significantly longer (200 km) than the estimated amount of south-directed shortening in
806 the eastern Southern Alps, which amounts to ≥ 50 km (Schönborn, 1999; Nussbaum, 2000). One way
807 to explain the excess slab length was also to take into account some 85 km of Miocene N-S
808 shortening accommodated in the Eastern Alps and some 55 km Miocene shortening taken up at the
809 front of the northernmost Dinarides (Ustaszewski et al., 2008, their fig. 6). Another way was to
810 assume that the eastern part of the slab is partly of European origin (Handy et al., 2015). Indeed,
811 recent models based on pre-AlpArray seismological data have combined ambient noise and P-wave
812 tomography to propose that Eastern Alps slab is actually a composite of predominantly European
813 lithosphere and a subordinate amount of Adriatic lithosphere (Kästle et al., 2020).

Deleted: transition

815 Our new results clearly show that there is only one slab below the Alps, rather than the two
 816 proposed by adherents of a switch in subduction polarity. A switch in the polarity of subduction
 817 beneath the Alps can thus be ruled out based on our new data. The notion of only one continuous
 818 European slab beneath the Alps was previously advanced by Mitterbauer et al. (2011), with the
 819 added observation that this slab is overturned and acquires a northward dip in the Eastern Alps, as
 820 also noted in our profiles (Fig. 4). A comparison of profiles across the Eastern Alps between the
 821 model of Lippitsch et al. (2003) in Fig. 10A and this work (Fig. 10B) demonstrates the poor fit of the
 822 models and highlights why mantle delamination and slab detachment rather than a change in
 823 subduction polarity are the most recent processes to leave their imprint in the Eastern Alps. The
 824 most striking difference, apart from the length of the slab, is that the detached European slab
 825 according to our model has no connection to the Adriatic lithosphere from which it is separated by
 826 low-velocity upper mantle (Fig. 10B).
 827



828
 829 **Figure 10:** Two tomographic profiles along the trace of profile C (given in inset map) on the same scale: (A)
 830 Lippitsch et al. 2003; (B) this work. The profiles show moderate agreement regarding slab detachment beneath
 831 the Eastern Alps, but disagreement regarding the dip and length of the slab anomaly. Our preferred model in (B)
 832 provides evidence for delamination of most of the underpinnings of Adria and Europe beneath the Alps, Adria and
 833 Apennines. A direct connection of the NE-dipping slab beneath the Eastern Alps to the Adriatic lithosphere shown
 834 in (A) becomes untenable in light of the new data presented in (B).
 835

Deleted: Yellow line in (B) is the outline of the slab anomaly in (A). The

838 The length of the slab measured in profiles varies along strike between 220 and ≥ 500 km,
839 with even the latter estimate regarded as a minimum, given that in some profiles the positive
840 anomalies continue below the 410 km discontinuity into the Mantle Transition Zone (e.g., profile 8
841 in Fig. 3A and profiles 6, 8, A and C in Appendix A). These lengths are not a reliable measure of the
842 amount of subducted lithosphere, because the slabs appear to be highly deformed and, anyway,
843 resolution decreases at such depths (Foulger, 2013). Nevertheless, the range of lengths overlaps
844 with palinspastic estimates of the total width of the Alpine Tethyan domain and its continental
845 margins in the Alps subducted between 84 and 35 Ma as measured in a NNW-SSE direction parallel
846 to Adria-Europe convergence (350-400 km, Le Breton et al., 2021; van Hinsbergen et al., 2020; 500
847 km, Handy et al., 2010). An interesting implication of this overall consistency between subducted
848 and seismically imaged lithosphere is that potentially more of the Alpine subduction is preserved in
849 the mantle than hitherto believed. Based on earlier teleseismic tomography, Handy et al. (2010)
850 estimated a deficit between subducted and imaged lithosphere of between 10 and 30%, depending
851 on the contour intervals of positive P-wave anomalies used in their areal assessments of positive
852 anomalies.

853 The steep northward dip of the part of the European slab beneath the Eastern Alps must
854 have been acquired after southward subduction of the European lithosphere stopped in this part of
855 the Alps. The youngest exhumed high-pressure rocks that are testimony to an exhumed subduction
856 zone in this part of the Alps are found in the central Tauern Window (Gross et al., 2000) and the age
857 of subduction-related metamorphism is estimated to be around 35-45 Ma (Kurz et al., 2008;
858 Ratschbacher et al., 2004 and refs. therein). A younger age range for this metamorphism was
859 proposed (32-35 Ma, allanite U-Pb, Smye et al. 2011; Lu-Hf, Nagel et al., 2013), but these are
860 inconsistent with evidence for substantial exhumation of high-pressure units before the intrusion of
861 the Periadriatic plutons and the onset of movements along the Periadriatic Fault System
862 (Rosenberg, 2004). The 35-45 Ma age range for HP metamorphism certainly pre-dates indentation
863 of the eastern Southern Alps along the Giudicarie Belt starting at around 23 Ma (Scharf et al., 2013).
864 Hence, roll back and steepening of the European slab, followed by slab detachment and rotation of
865 the detached Eastern Alps slab into a steeply N-dipping orientation most likely occurred sometime
866 within the 39-23 Ma time interval, most likely at around 23 Ma according to geological evidence
867 (e.g., Scharf et al., 2013). The mechanisms of such rotation and verticalization during opening of the
868 Pannonian backarc behind the European slab subducting beneath the Eastern Carpathians are
869 unclear. The slab might have been twisted while still attached to a descending slab relict beneath
870 the Pannonian Basin (profile 5 in Fig. 5B; Dando et al., 2011). However, we favor reorientation of
871 the slab by asthenospheric flow during or after northward Adriatic indentation and slab detachment
872 in Neogene time (e.g., Ratschbacher et al., 1991; Favaro et al., 2017). The arcuate convex-
873 northward pattern of fast SKS directions beneath the Eastern Alps are suggestive of east-directed
874 asthenospheric flow (e.g., Qorbanli et al., 2015) and would be consistent with both of these
875 interpretations.

876 6.2 Slab attachment and detachment

877 An intact slab dipping down to a depth of 300 km and beyond is only observed beneath the Western
878 to Central (Swiss-Italian) Alps between latitudes 7°E and 10°E (see area marked as un-detached in
879 Fig. 8; profiles 6 and 9 in Appendix A. Interestingly, Singer et al. (2014) noticed that lower crustal
880 seismicity in the European lithosphere is restricted to this same range of latitudes. They proposed
881 that this deep crustal seismicity is driven by stresses transferred to the foreland from the still-
882 attached segment of the European slab, which they argue is steepening as it retreats toward the
883 foreland. Kissling and Schlunegger (2018; their fig. 5c) present a schematic 3-D diagram of this

Deleted: s

Deleted: a

Deleted: ,

888 remaining undetached European slab, arguing that such slab retreat during attachment is
889 responsible for the striking isostatic disequilibrium between the low surface topography and the
890 thick crustal root (some 50 km, e.g., Spada et al. 2013) beneath this segment of the Alps.

Deleted: e

891 Complete delamination during the advanced stages of detachment of the European
892 lithosphere occurred in the Eastern Alps and resulted in a broad zone of low-velocity material
893 interpreted to be upwelling mantle (Fig. 9), typically at a depth between 70 and 130 km (e.g., profile
894 15 in Fig. 5A) east of 12°E (i.e., east of the western Tauern Window, Fig. 1). East of 15°E, no
895 substantial remnants of the European slab are found above the 410 km discontinuity (Fig. 8 and
896 profiles 5, 11, 10 in Appendix A). This conforms with the findings of Dando et al. (2011) and
897 indicates that roll back subduction in the Carpathians followed by detachment of the European slab
898 played a fundamental role in forming the greater Pannonian area (Horvath et al., 2006; Matenco
899 and Radivojević, 2012). West of the Tauern window, between 12° and about 9.5°E traversed by
900 profile B (Fig. 3C), detachment is only moderate. A third area in the Alps where substantial
901 detachment occurs is the southern part of the Western Alps (profiles 8 in Fig. 3A, and A in Appendix
902 A) that is transitional to the northern Apennines. Such detachment was first noticed by Lippitsch et
903 al (2003; their profile A-A'), but recently refuted by Zhao et al. (2016). There, the detached
904 European slab of the Alps slab resides beneath the westernmost Apennines at a depth of 240 km,
905 while upwelling mantle occupies the area beneath the Western Alps at this same depth (Fig. 8).

906 The completely detached slab beneath most of the Northern Apennines (except for the
907 westernmost parts) hangs subvertically (profiles 11 and 12 in Fig. 6; profile C in Appendix A),
908 confirming the findings of Giacomuzzi et al. (2011, 2012) from teleseismic tomography, but at odds
909 with the interpretation of still-attached continental slabs without oceanic precursors in Sun et al.
910 (2019). A clear boundary between the European slab under the westernmost Apennines and the
911 delaminated Adriatic mantle lithosphere of the Northern Apennines slab cannot be resolved in the
912 horizontal depth slices, but is evident in profiles (e.g., Fig. 3A), where we interpret the boundary
913 between the two slabs to coincide with the Alpine Tethys suture.

914 6.3 Nature of low velocity domains in the greater Alpine area

915 In the text and profiles above, we interpret low V_p areas within the Circum-Adriatic area as resulting
916 from upwelling mantle material (Pannonian Basin, Eastern Alps) and hydration effects (Veneto
917 Basin), whereas negative V_p areas in the lower part of the European lithosphere reflect inherited
918 Variscan or pre-Variscan structural anisotropy and/or compositional differences rather than
919 enhanced temperature (section 4).

Deleted: c

920 Insight into the nature of the European lithosphere comes from the striking coincidence of
921 its lower layer of large $-V_p$ anomaly (Figs. 2, 7) with NE-SW oriented SKS directions and 1-2s delay
922 times reported for this area in the literature (Barruol et al. 2011) and AlpArray studies (Link and
923 Rumpker, pers. comm.). Given a relation of 100 km thickness for every second of delay time, one
924 obtains a thickness of 100-200 km for the anisotropic layer, which matches the observed thickness
925 of the $-V_p$ layer. A well-known effect of azimuthal anisotropy is to retard near-vertical-incident body
926 waves (Hammond, 2014; Munzerová et al., 2018), thus providing a possible explanation for the
927 anomalous $-V_p$ layer. Taken together, this suggests that the $-V_p$ layer in the lower European
928 lithosphere is structurally anisotropic and may have accommodated viscous flow. This is contrary to
929 previous interpretations in which the anisotropy was attributed to arc-parallel asthenospheric flow
930 around the European slab (Barruol et al., 2011). The NE-SW orientation of SKS directions below the
931 Central Alps is inconsistent with the SE-subduction direction of European lithosphere, leaving a
932 Variscan or pre-Variscan age for lower lithospheric flow as the most likely alternative.

933 We consider a thermal anomaly unlikely to have caused the large $-V_p$ anomaly in the
934

937 European lithosphere because the ΔT -values corresponding to the observed 5-6% $-V_p$ would be
938 unrealistically high (300-600°C using the ΔV_p -T relations of Goes et al., 2000; Cammarano et al.,
939 2003; Perry et al., 2006) for old, inactive mantle lithosphere in the down-going plate of a collisional
940 orogen. Variscan crust in the foreland of the Alps underwent amphibolite- to locally granulite-facies
941 regional metamorphism some 340-360 Ma ago, followed by calc-alkaline magmatism and thermal
942 overprinting at 320-260 Ma (e.g., Matte 1986; Franke, 2000 and refs. therein). This Late
943 Carboniferous to Early Permian magmatic event is at least 200 Ma older than the onset of collision
944 in the Alps at 40-32 Ma (e.g., Handy et al., 2010 and refs. therein). Though it has been argued that
945 compositional differences can stabilize vertical and horizontal thermal gradients (Jordan 1975,
946 1981), thus contributing to the longevity of the observed seismic heterogeneity, there is no known
947 mechanism to maintain such a pronounced thermal anomaly for such a long time.

948 Regarding the Adriatic Plate, the question remains if the younger, low V_p patches attributed
949 to Miocene asthenospheric upwelling following lithospheric delamination (Fig. 9) still represent
950 volumes of substantially elevated temperatures today. In view of the fact that water content in
951 addition to temperature influences seismic wave velocities in the mantle (Karato and Jung, 1998;
952 Shito et al., 2006), we propose that at least in the case of the Veneto volcanic province (Fig. 8)
953 temperature is unlikely to be the dominant factor, especially given that present-day heat flow in the
954 Adriatic region is low (Giacomuzzi et al., 2011).

955 956 6.4 Timing of slab detachment and its geodynamic consequences

957 A rough estimate of the time since slab detachment in the Eastern Alps can be obtained from the
958 average sink rate of slabs around the world (12 mm/a, van der Meer et al., 2010, 2018). The rate is
959 derived from a compilation of teleseismically imaged slabs of known lengths and ages that are still
960 attached to their lower plate lithospheres, mostly in Circum-Pacific convergent zones. When applied
961 to the Eastern Alps, this approach yields minimum values of the time since detachment because
962 delamination of the European lithosphere is inferred to have preceded slab detachment (Figs. 4 and
963 6). They range from 10 to 25 Mas, respectively, beneath the Eastern Alps and the Pannonian Basin.
964 The 10-25 Ma time range since slab detachment encompasses the period of orogen-parallel
965 extension and rapid exhumation and lateral escape in the Tauern Window (23-11 Ma, e.g., Scharf et
966 al., 2013) and overlaps with the duration of extension in the Pannonian Basin (21-15 Ma, Horvath et
967 al., 2015 and references therein). This supports our suggestion that lithospheric delamination, slab
968 detachment and asthenospheric upwelling were instrumental in triggering decoupling that enabled
969 Neogene orogen-parallel lateral extrusion of the ALCAPA tectonic megaunit (upper plate crustal
970 edifice of Alps and Carpathians) towards the Pannonian Basin. This raises questions about the depth
971 of detachment at the base of the ALCAPA megaunit during its lateral extrusion and the nature of the
972 Moho beneath the Pannonian Basin. Horvath et al. (2015) proposed that during lateral extrusion the
973 extending crust of the ALCAPA megaunit directly overlay the hot asthenosphere of the Carpathian
974 embayment and that since then, most of the Pannonian Basin cooled, allowing a new mantle
975 lithosphere to accrete. If correct, this would imply that the Moho imaged beneath the Pannonian
976 basin is of Miocene or younger age.

977 An intriguing aspect of Adriatic indentation and Alpine slab detachment is their potential
978 effects on the fore- and hinterland basins of the Alps. The 25-10 Ma time window for slab
979 detachment brackets the time when thrusting in the eastern Molasse basin stopped advancing (21-
980 22 Ma) and changed from in-sequence to out-of-sequence (wedge-top) mode (Hinsch, 2013). It also
981 includes the time when the basin rapidly filled with terrigenous components at 19-18 Ma (Grunert
982 et al., 2013), leading to a shift in the paleo-drainage direction from eastward to northwestward
983 (Kuhlemann and Kempf, 2002). Subsequent uplift and erosion of the entire Molasse Basin at 10 to 5

Deleted: r

Deleted: could

Deleted: grow

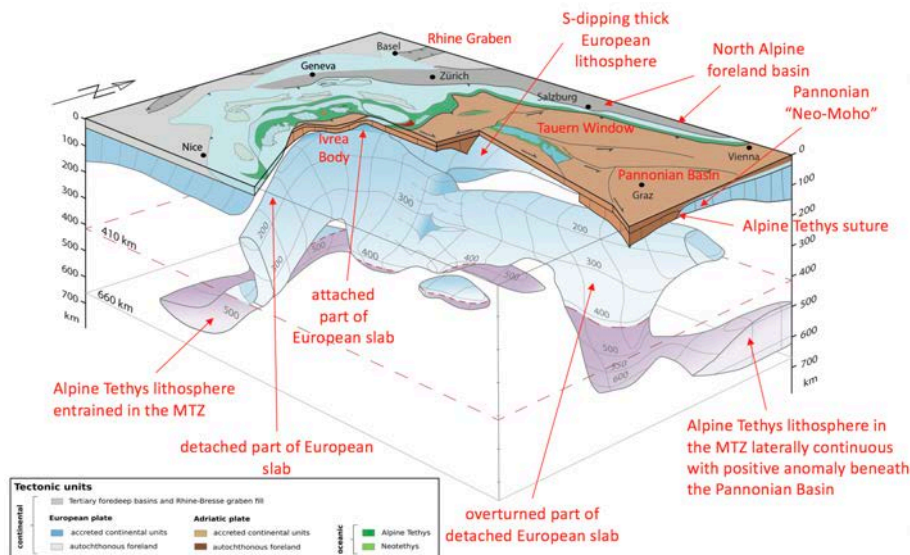
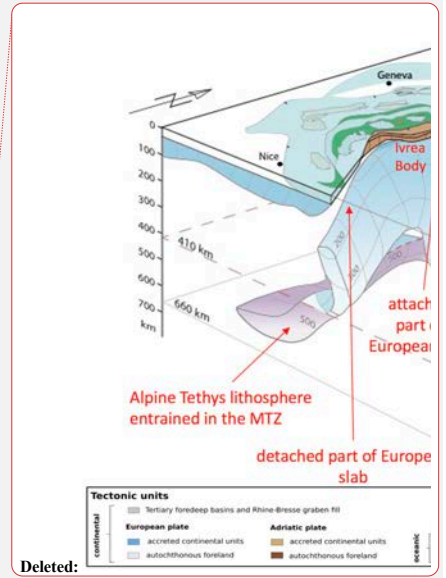


Figure 11: 3D-diagram of the slab beneath the Alps as viewed from the southeast. Slab geometry based on projections of all vertical tomographic profiles in Appendix B and horizontal sections from the model of Paffrath et al. (2021b). Tectonic map of the surface is simplified from maps of Schmid et al. (2004) and Schmid et al. (2008).

A prime outcome of this study is that the European and Adriatic Plates involved in Alpine collision have first-order differences in seismic structure: the down-going European lithosphere is thick (c. 180 km) and marked by laterally continuous positive and negative P-wave anomalies. These are believed to be inherited Variscan or pre-Variscan anisotropic and compositional differences. In the Central (Swiss-Italian Alps), they descend as part of a coherent slab from the Alpine foreland to beneath the Northern Alpine Front. In contrast, the Adriatic Plate is thinner (100-120 km) and has a poorly defined base at the lower boundary of $+V_p$ anomalies. The underlying negative anomaly in the depth interval of 120-270 km is attributable partly to compositional effects (e.g., mantle hydration due to upwelling fluids from the Alpine slab) and partly to upwelling asthenosphere in the aftermath of delamination and slab detachment in the Alps and Apennines.

This fundamental difference in the structure of the lower and upper plates may be responsible for two of the most striking features of the Alps compared to other Alpine-Mediterranean orogens, namely the rugged, high altitude Alpine topography and the disproportionately large amount of accreted, deeply subducted and exhumed lower-plate units exposed in the deeply eroded core of the Alps (Fig. 11). Thick lithosphere is expected to be relatively stiff and buoyant upon entering collision, favoring tectonic underplating of accreted and subducted tectonic units as subduction proceeds. By comparison, “normal” lithosphere, as found in the Adriatic Plate and its slab beneath the Apennines, is expected to sink more easily under its own weight, favoring roll-back subduction, the development of low topography and upper plate extension with only limited exhumation of subducted units.

Another new outcome of this study is the extent of delamination and detachment of slabs in both the Alps and the Apennines. Detachment is complete in the southwestern-most Alps, and on a



Deleted:

1042
1043
1044
1045
1046
1047
1048
1049
1050
1051
1052
1053
1054
1055
1056
1057
1058
1059
1060
1061
1062
1063
1064
1065
1066
1067
1068

1070 much larger scale, in the Eastern Alps (Fig. 11) and Western Carpathians. There, relicts of European
1071 lithosphere hang at various depths, with depth increasing towards the east and even reaching the
1072 MTZ beneath the Pannonian Basin. Large-scale upwelling of asthenosphere was the response of the
1073 mantle to delamination of the European lithosphere and downward motion of detached slabs since
1074 at least 25 Ma. The asthenosphere below delaminated lithosphere occupies very shallow depths, in
1075 some cases immediately below the Moho marking the base of thinned Alpine orogenic crust, which
1076 was stretched in Neogene time during lateral orogenic escape and upper-plate extension forming
1077 the Pannonian Basin.

1078 In this study, we claim to have resolved the debate over the polarity of Alpine subduction
1079 beneath the Eastern Alps in favor of a model with a single European slab that originally subducted
1080 to the south. The presently steep, northward dip of the now-fragmented and deformed Eastern Alps
1081 slab segment (Fig. 11) which gave rise to the alternative view of northward Adriatic subduction in
1082 the first place, is clearly a secondary feature acquired during or after slab detachment.

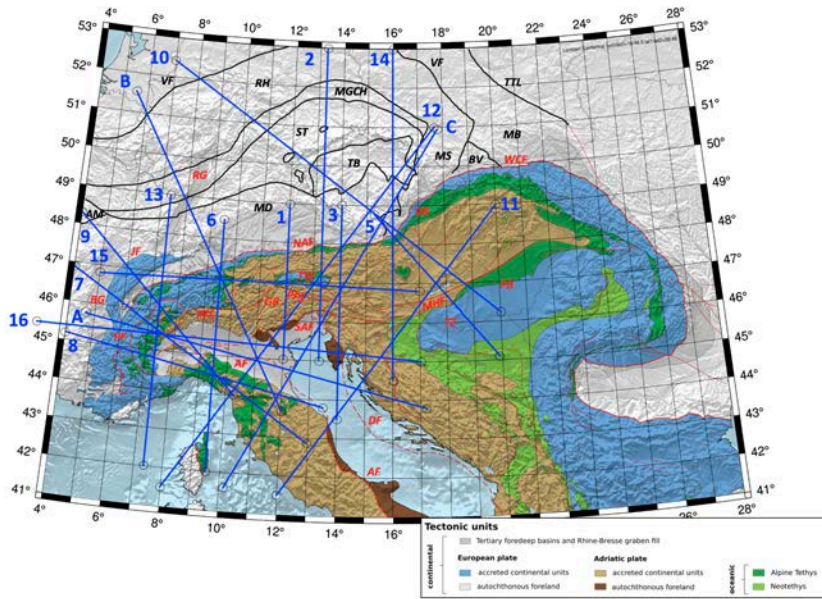
1083 A lesson learned in collating and interpreting this extraordinary data set has been that, after
1084 initially acquiring and processing seismological data, methodological development and tectonic
1085 interpretation must go hand-in-hand if they are to yield meaningful, testable models. Figure 11 is an
1086 initial model of tectonic boundaries based on an assessment of geophysical data in a plate
1087 kinematic context. The next step is obviously to parameterize this model in order to compare it with
1088 independent sources of data and determine its thermo-mechanical characteristics.

1089
1090
1091

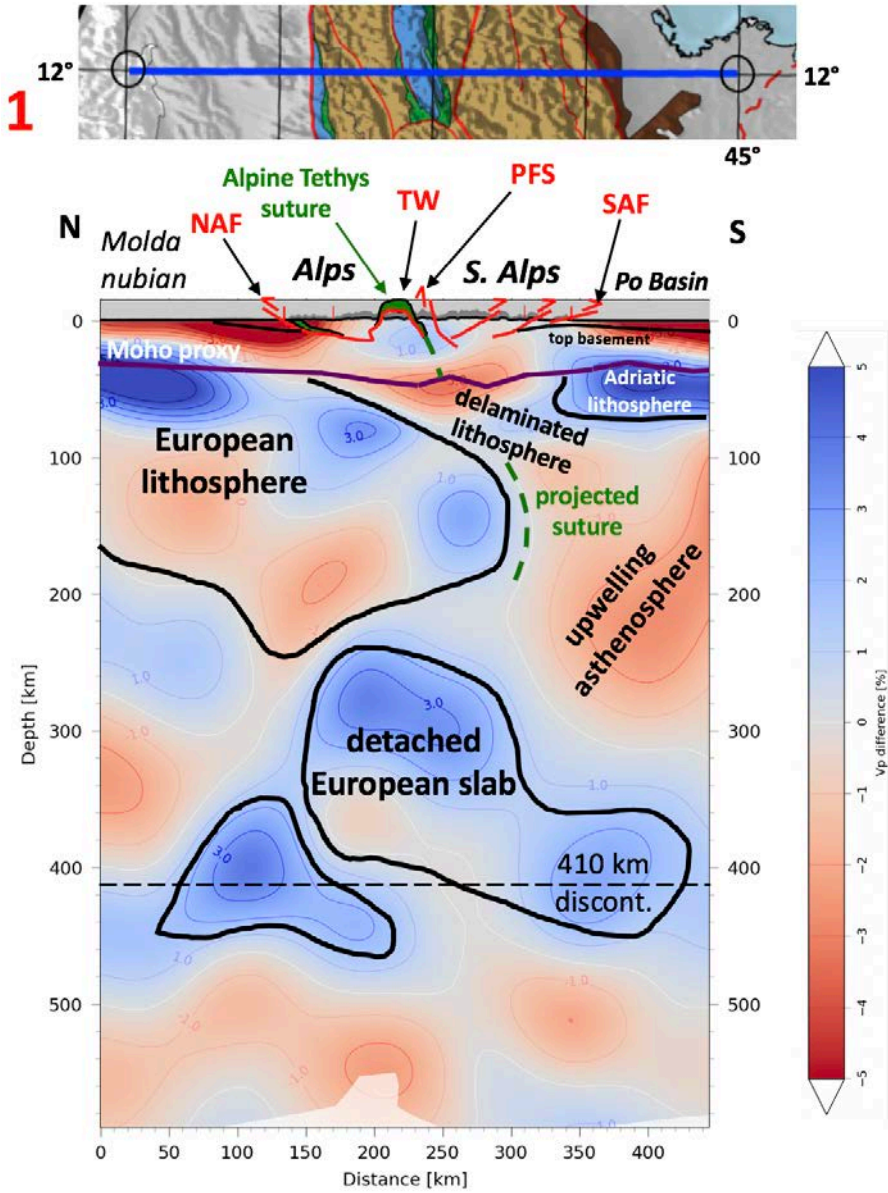
Deleted: the

Deleted: of

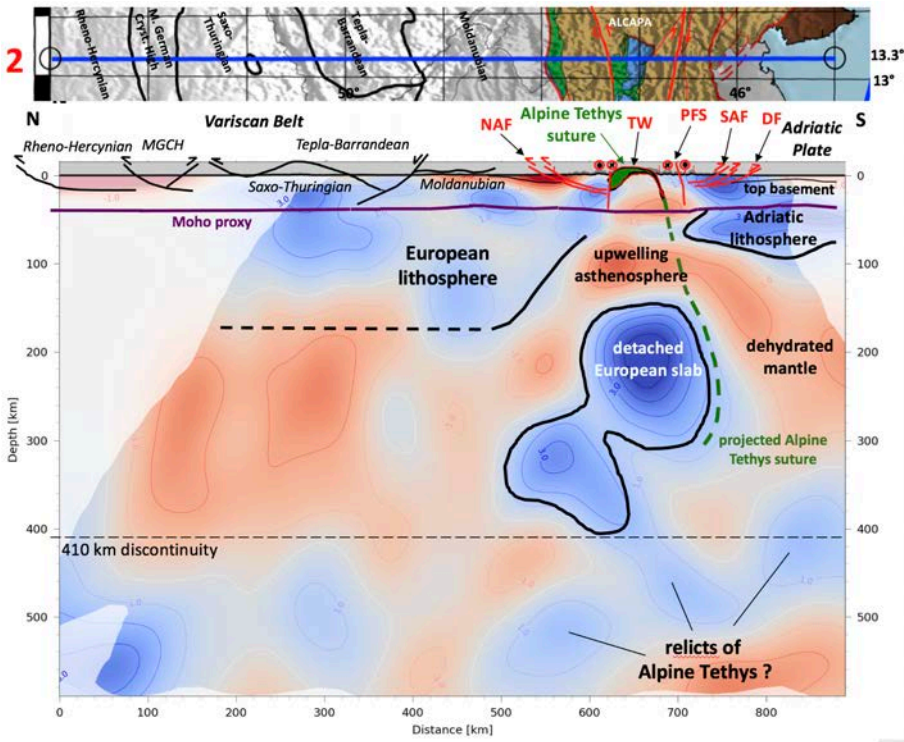
1094 **Appendices**
 1095
 1096 Profiles used in interpretations
 1097



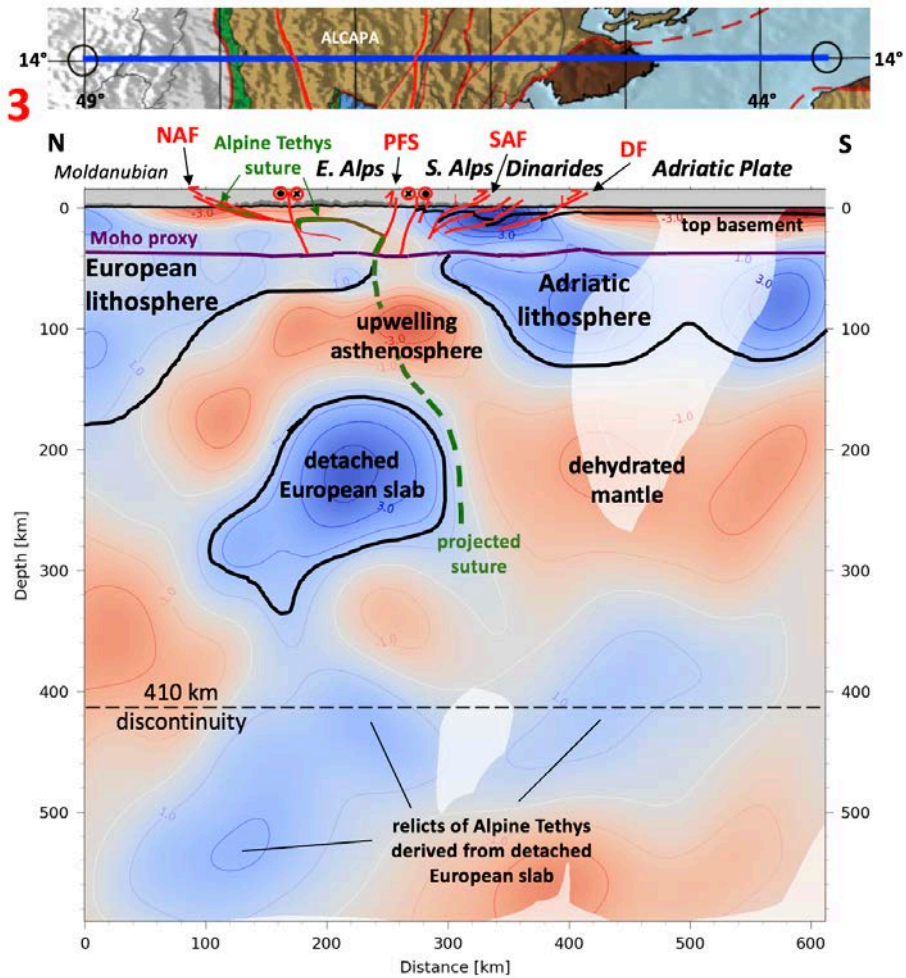
1098 Fig. A0 Tectonic map with traces of all tomographic profiles used in this study
 1099
 1100



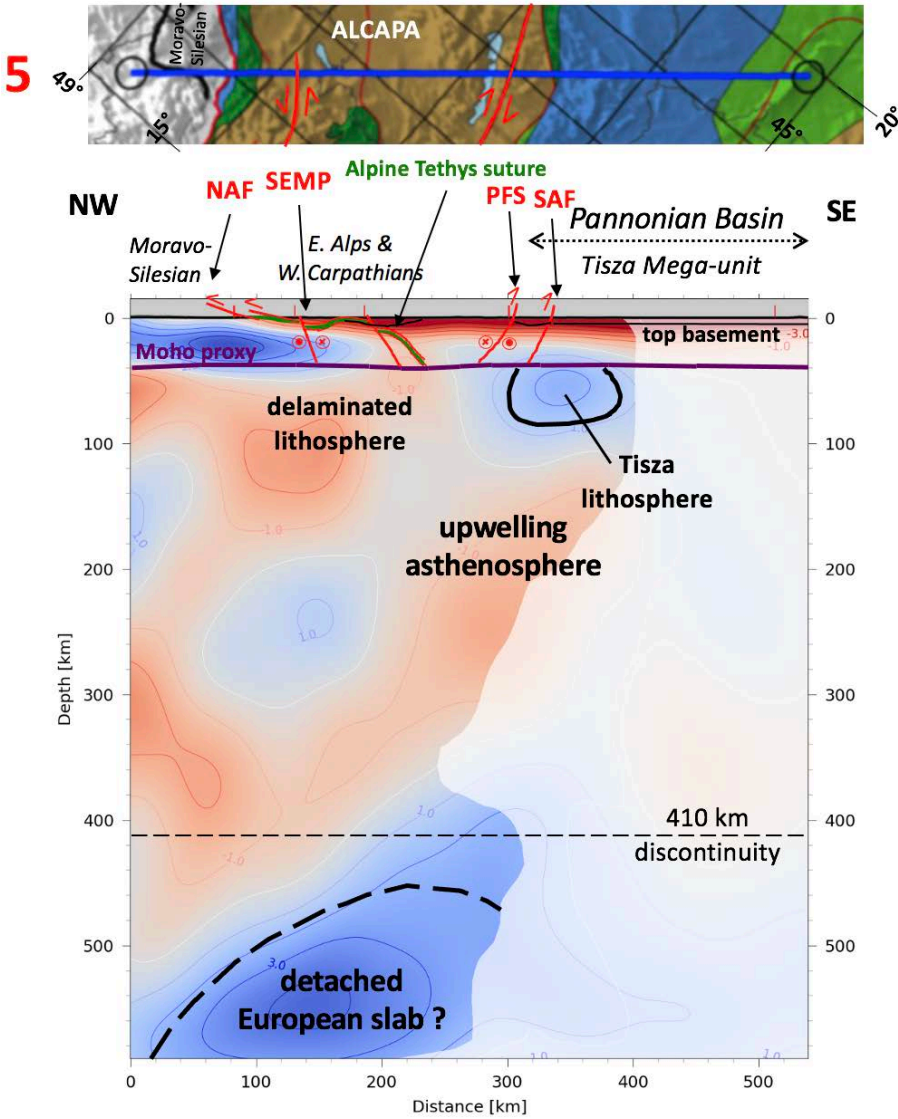
1101
1102 Fig. A1 Profile 1



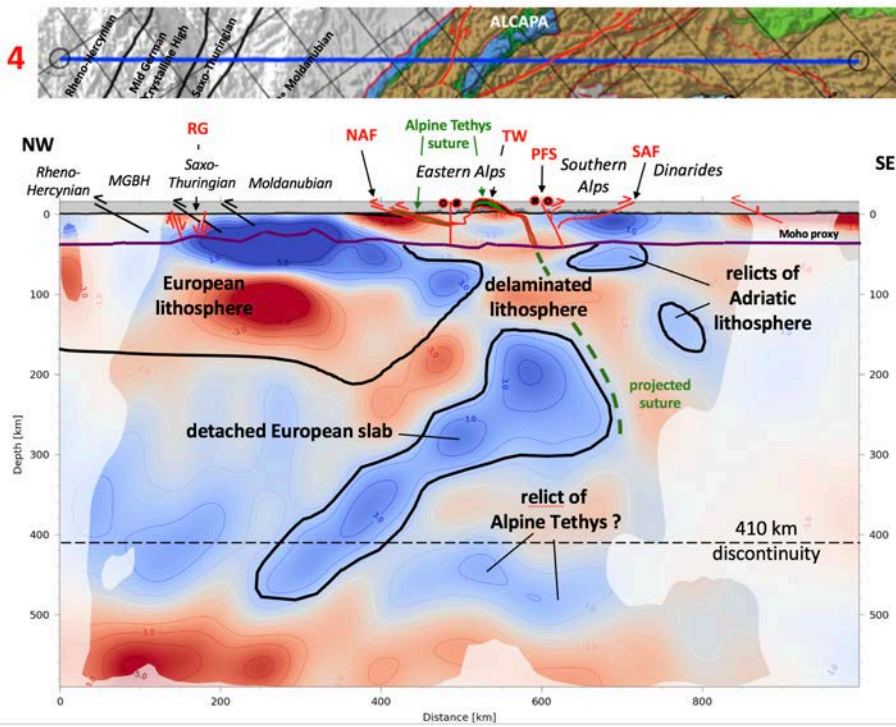
1103
1104 Fig. A2 Profile 2



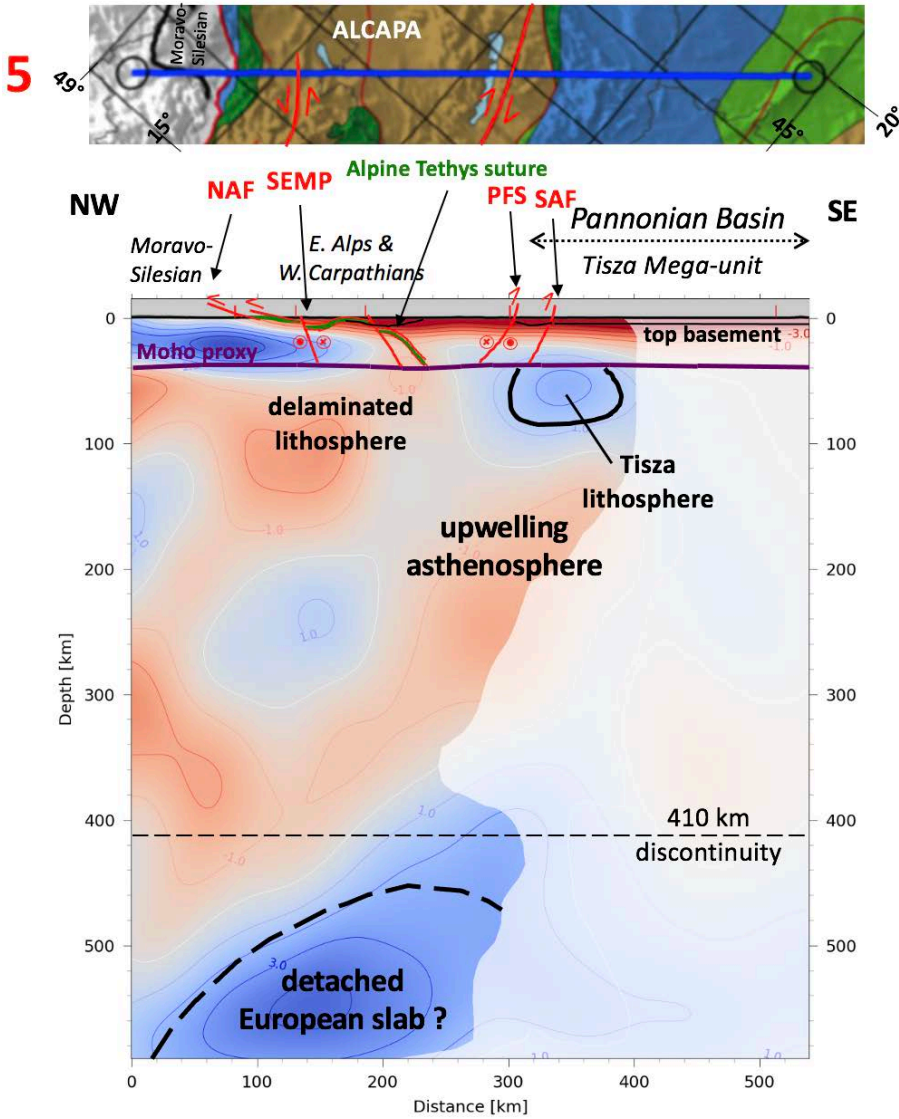
1105
1106 Fig. A3 Profile 3



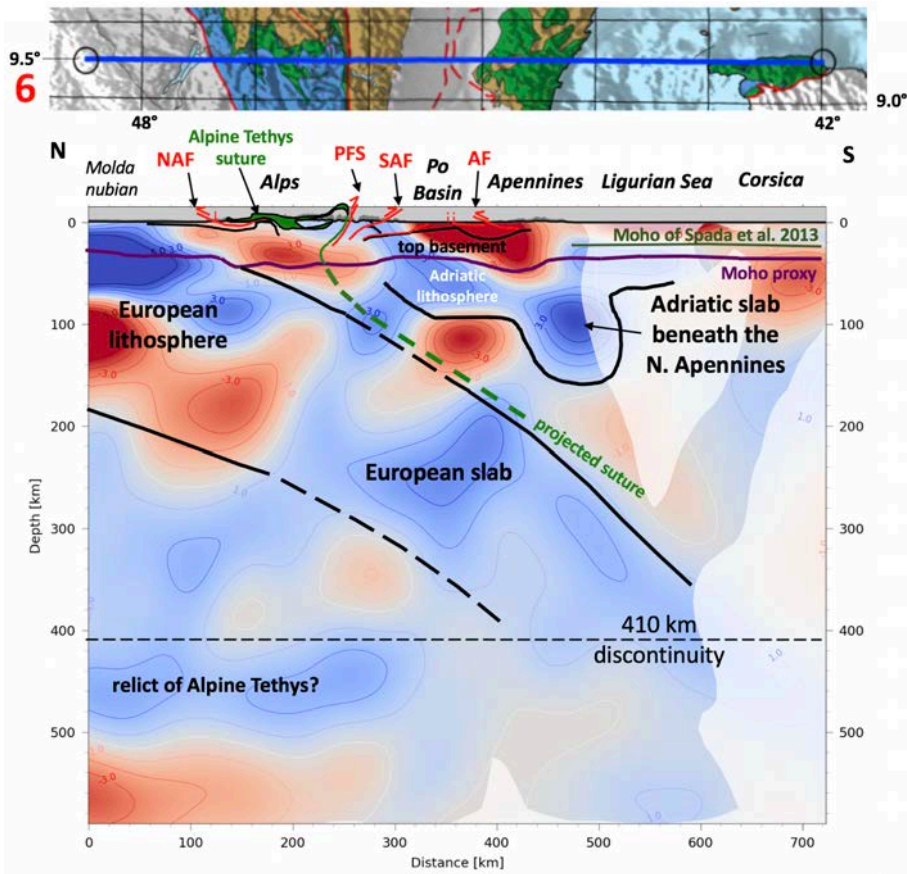
1107



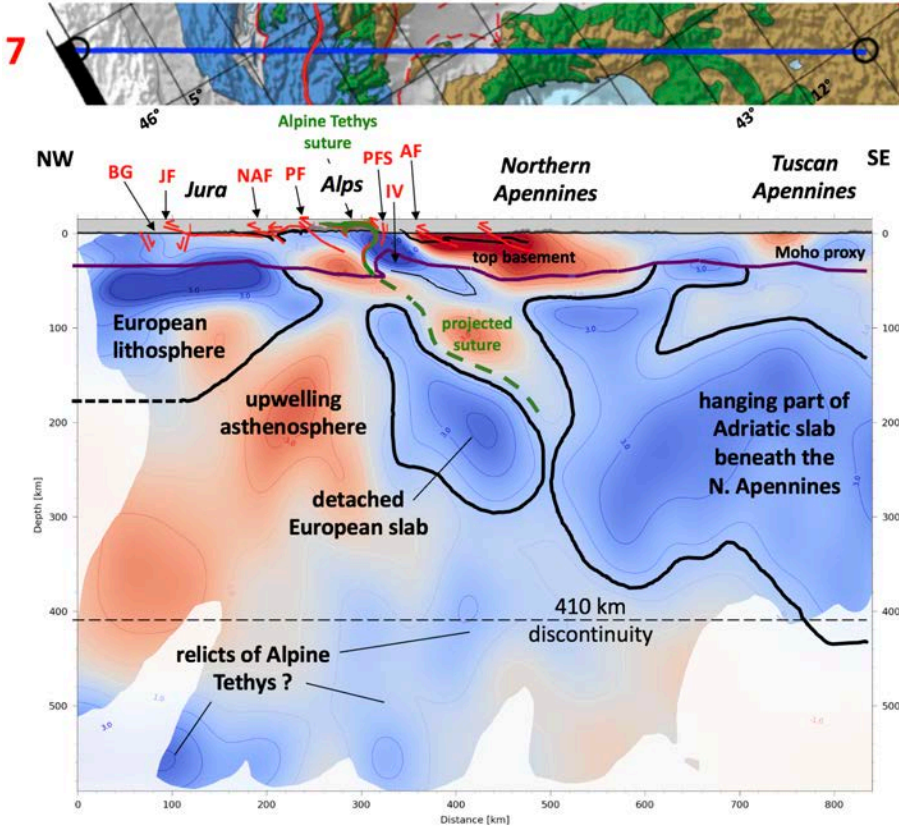
1108
1109 Fig. A4 Profile 4



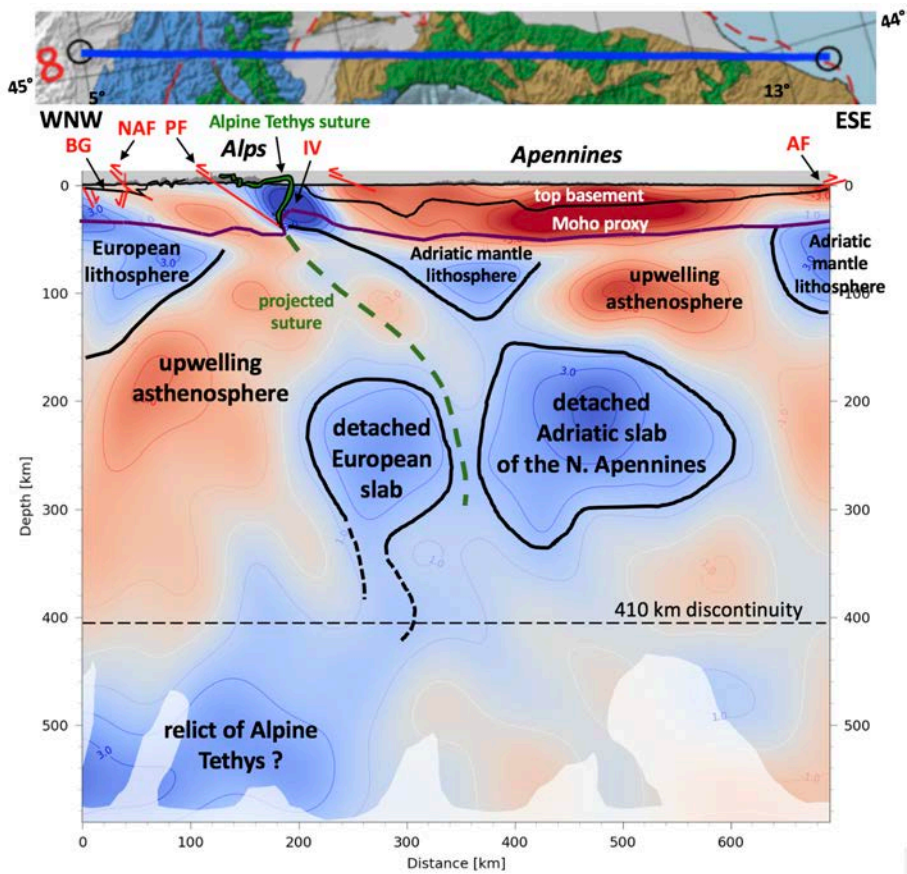
1110 Fig. A5 Profile 5
1111



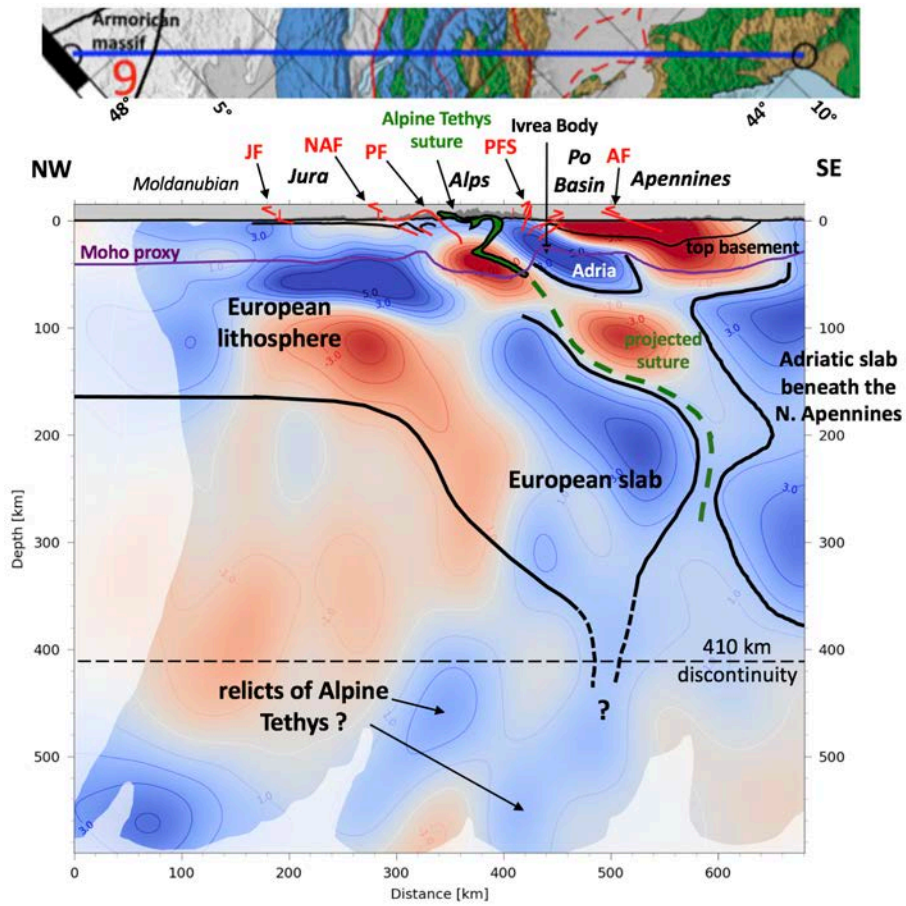
1112
1113 Fig. A6 Profile 6



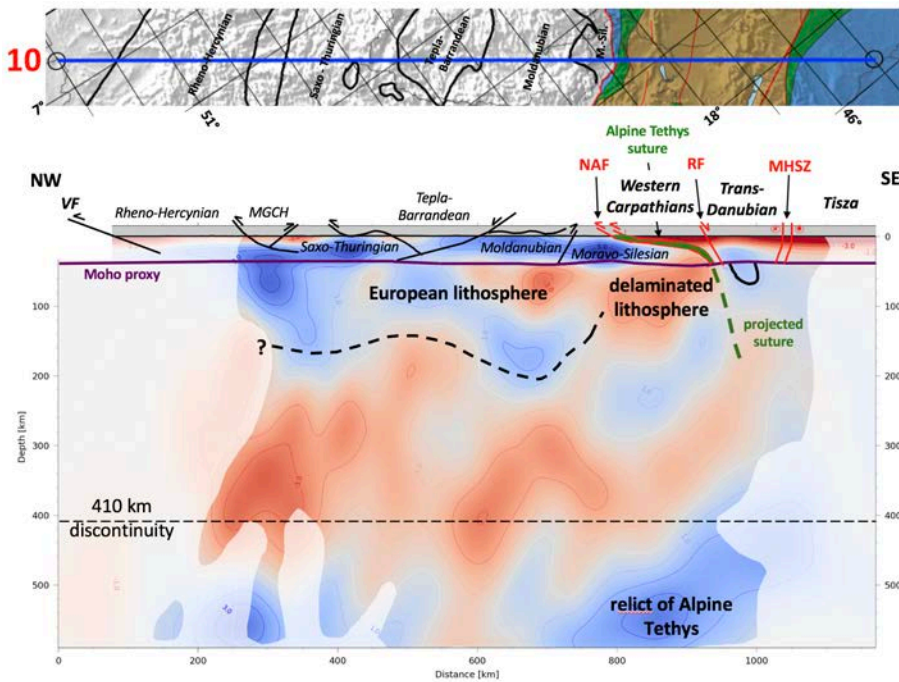
1114
1115 Fig. A7 Profile 7



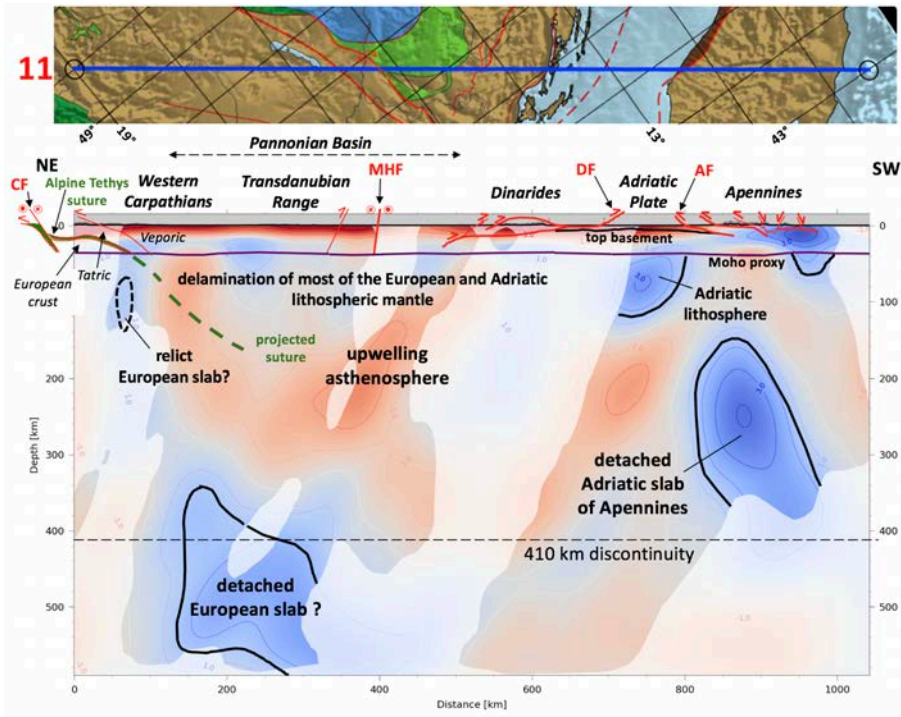
1116
1117 Fig. A8 Profile 8



1118
1119 Fig. A9 Profile 9

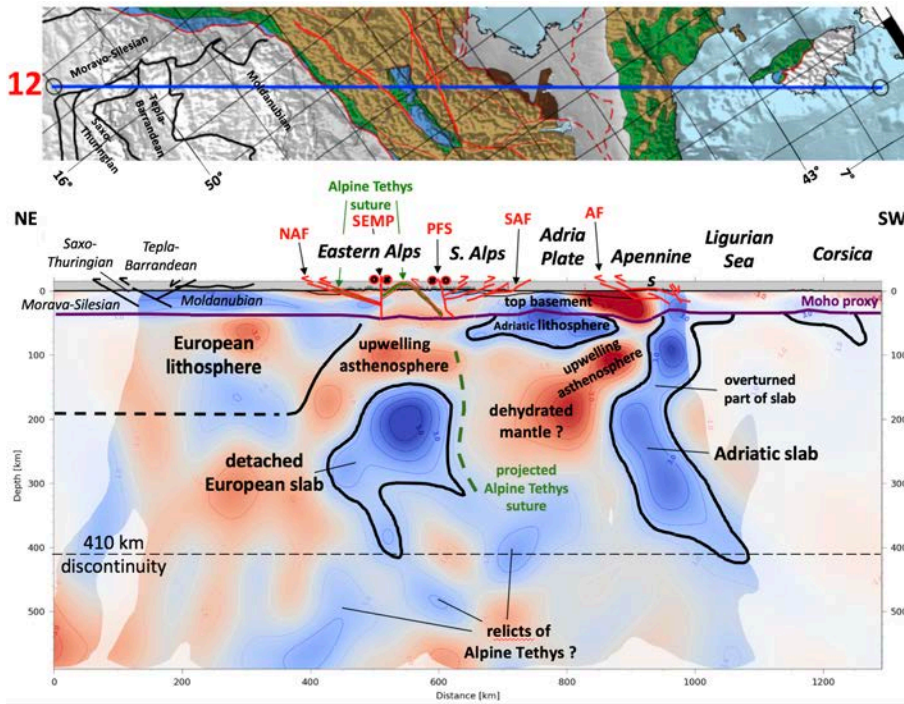


1120
1121 Fig. A10 Profile 10

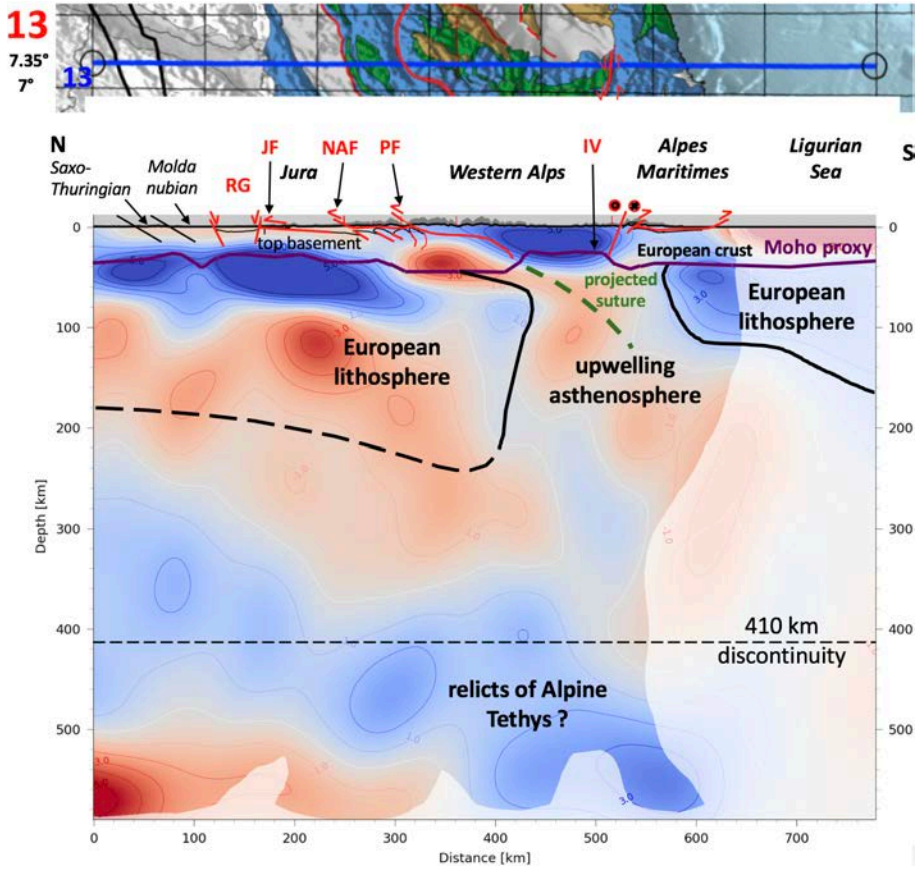


1122
1123

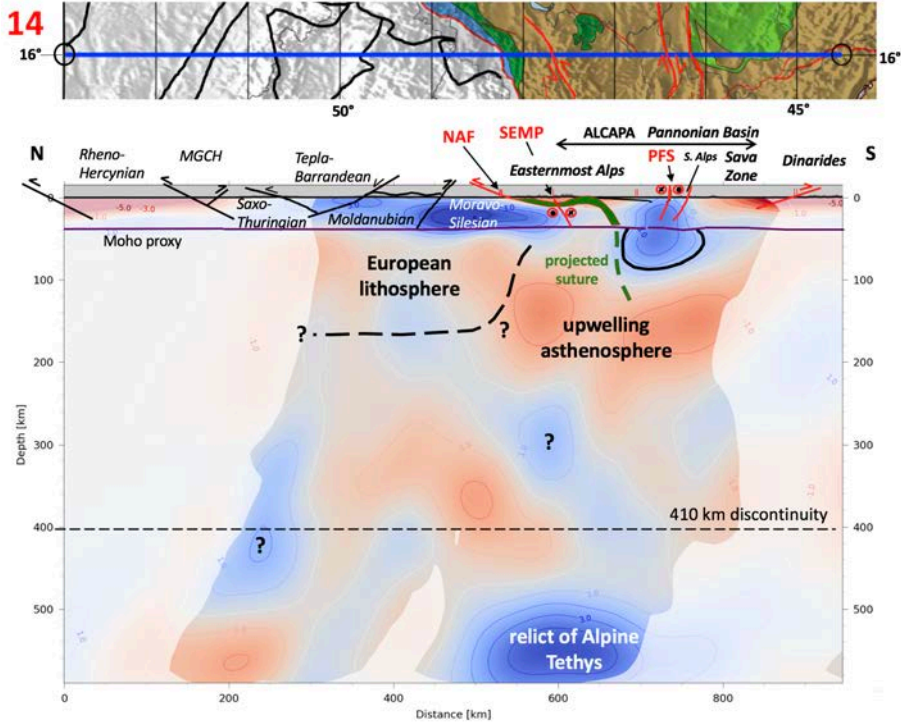
Fig. A11 Profile 11



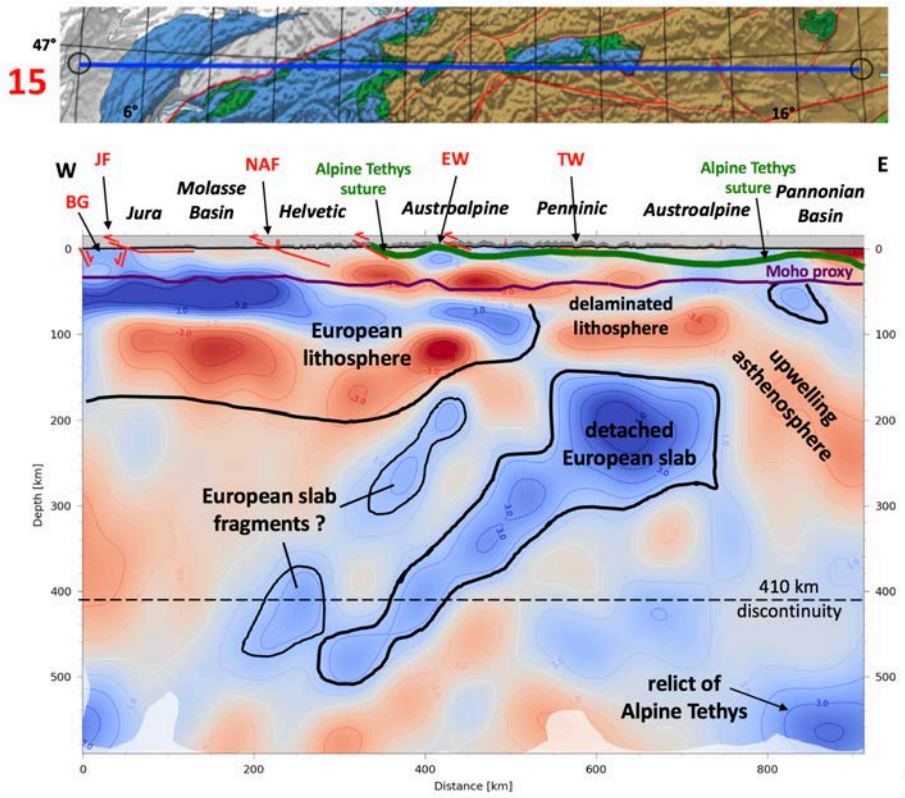
1124
1125
1126
Fig. A12 Profile 12



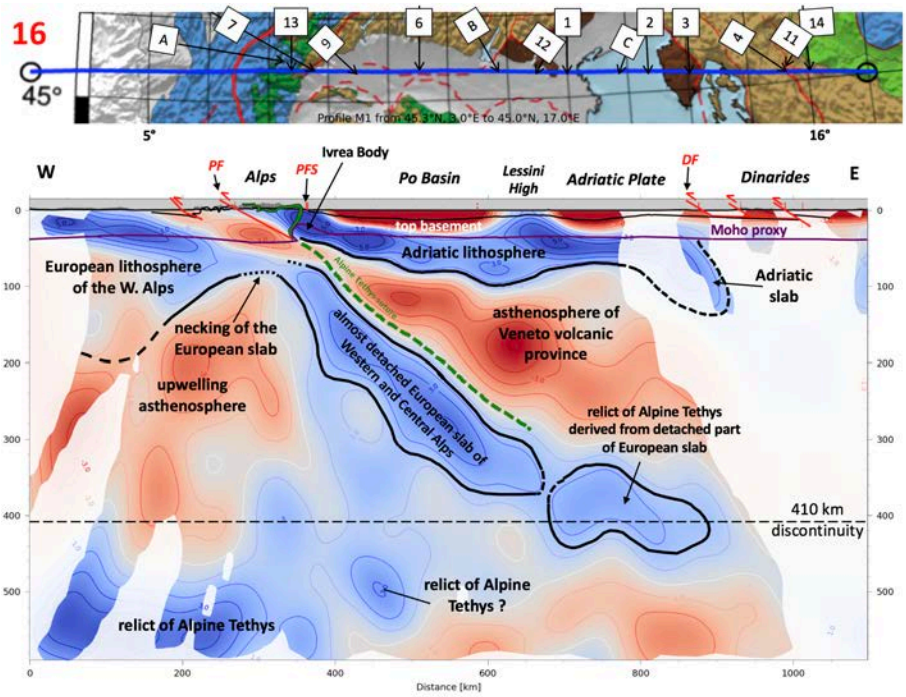
1127
1128 Fig. A13 Profile 13
1129



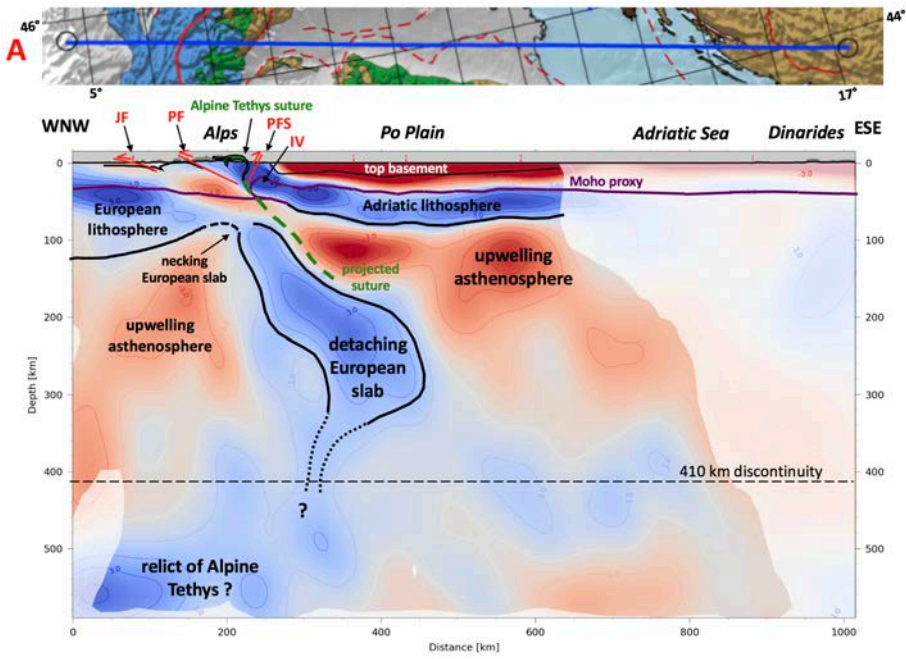
1130 Fig. A14 Profile 14
 1131
 1132



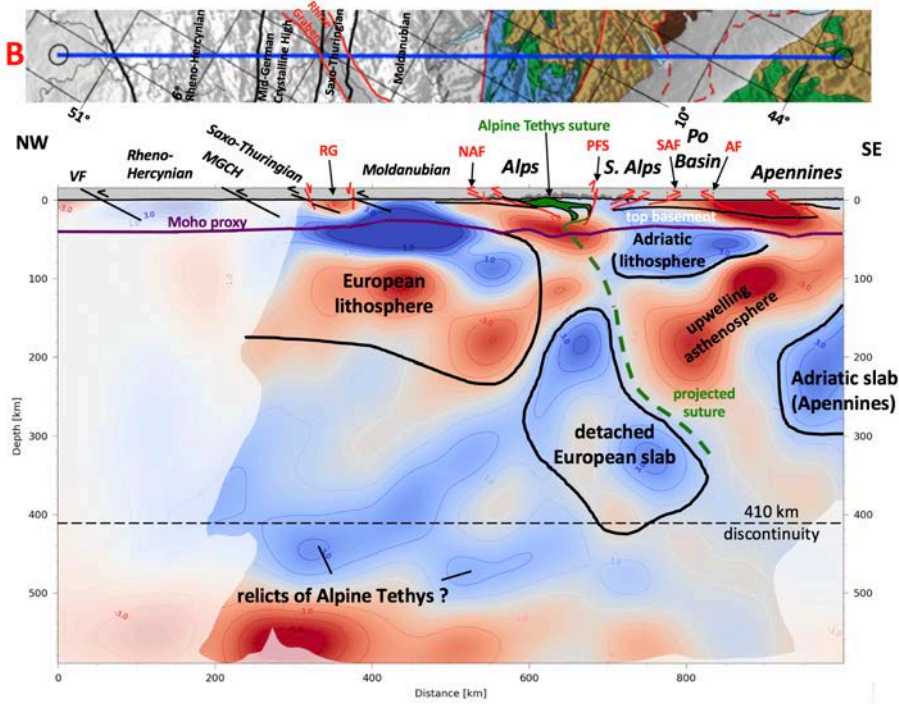
1133
1134 Fig. A15 Profile 15
1135



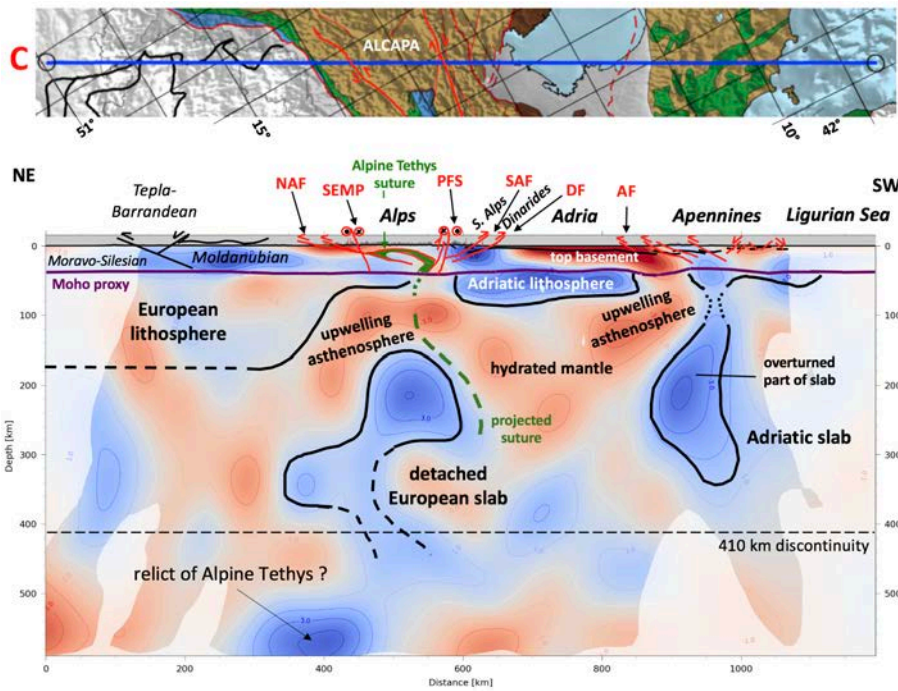
1136
 1137 Fig. A16 Profile 16. Numbered labels at top indicate intersecting profiles.
 1138



1139
 1140 Fig. A17 Profile A
 1141

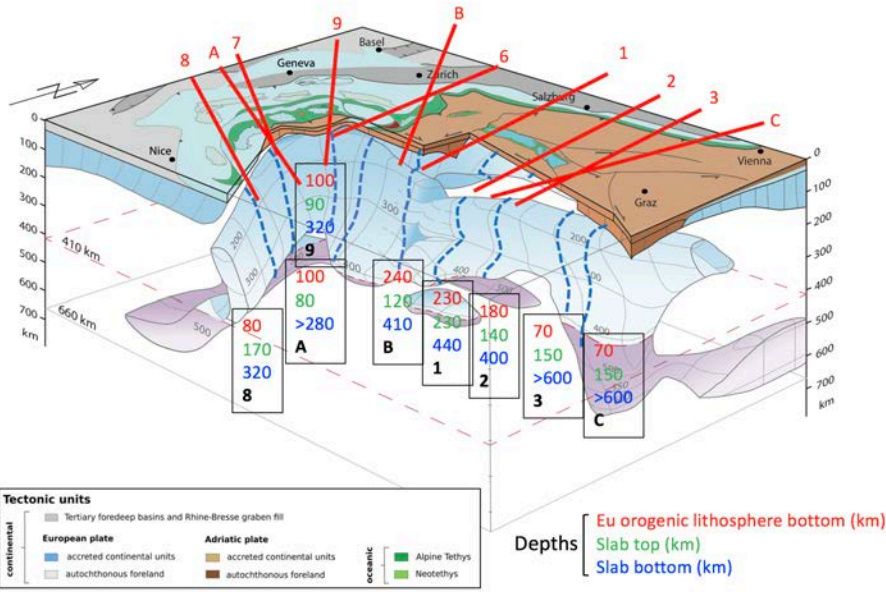


1142
 1143 Fig. A18 Profile B
 1144



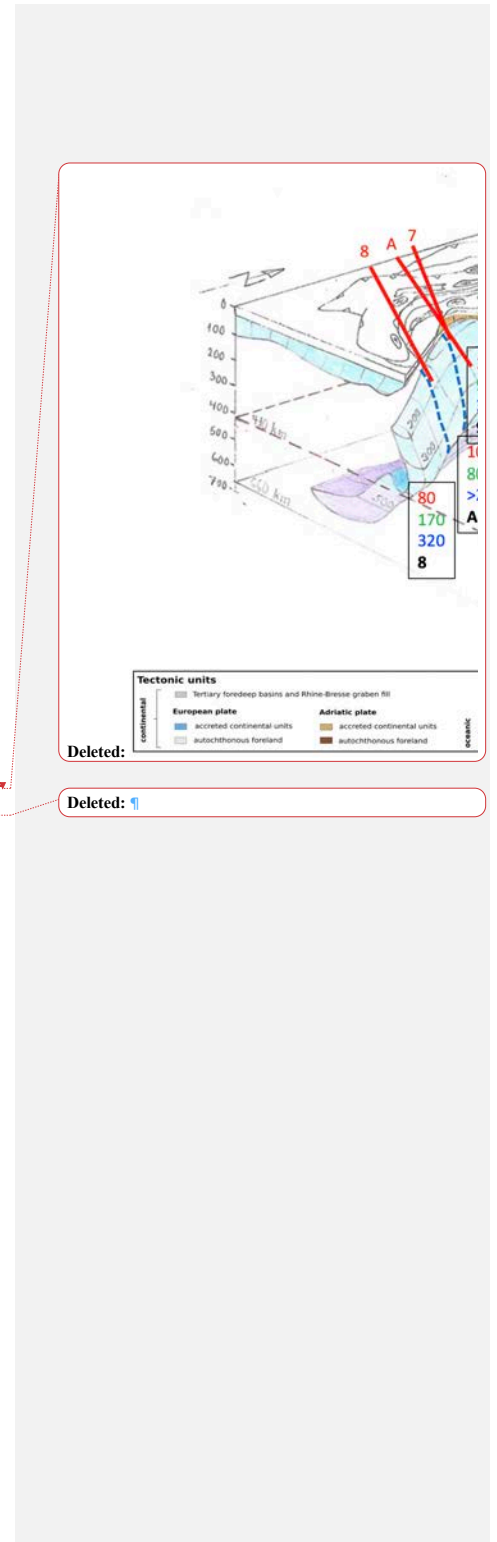
1145
 1146 Fig. A19 Profile C
 1147
 1148

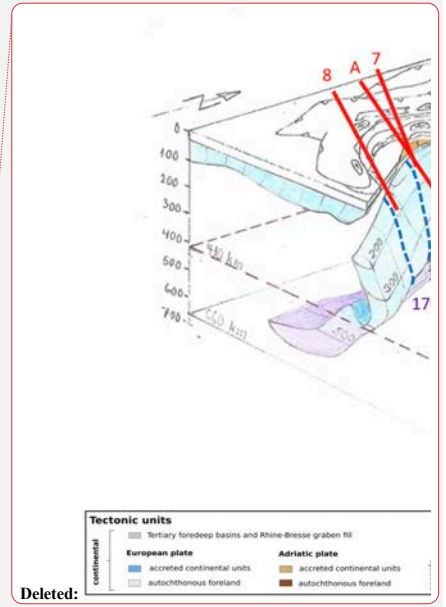
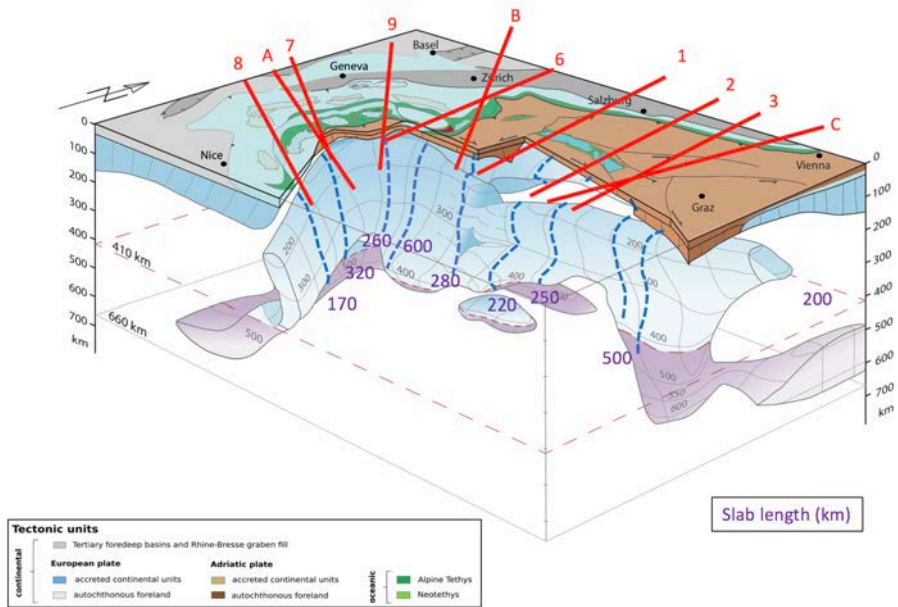
1149



1150
1151
1152
1153

Fig. B1 3D block diagram with depths to slab tops and bottoms





1156
 1157 Fig. B2 3D block diagram with slab lengths
 1158
 1159
 1160
 1161
 1162
 1163
 1164

1166 **Team List**

- 1167 1. Mark R. Handy - Institut für Geologische Wissenschaften, Freie Universität Berlin, Malteserstr.
1168 74-100, 12249 Berlin, Germany; Institut für Geologie, ETH-Zürich, Sonneggstr. 5, 8092 Zürich
1169 2. Stefan M. Schmid - Institut für Geophysik, ETH-Zürich, Sonneggstr. 5, 8092 Zürich
1170 3. Marcel Paffrath - Institut für Geologie, Mineralogie, Geophysik, Ruhr-Universität Bochum, 44780
1171 Bochum, Germany
1172 4. Wolfgang Friederich - Institut für Geologie, Mineralogie, Geophysik, Ruhr-Universität Bochum,
1173 44780 Bochum, Germany
1174 5. AlpArray Working Group: [http://www.alparray.ethz.ch/en/seismic_network/backbone/data-](http://www.alparray.ethz.ch/en/seismic_network/backbone/data-policy-and-citation/)
1175 [policy-and-citation/](http://www.alparray.ethz.ch/en/seismic_network/backbone/data-policy-and-citation/).

1176

1177 **Author contributions**

1178 Mark Handy and Stefan Schmid interpreted the tomographic profiles and slices that were provided in
1179 raw form by Marcel Paffrath. The latter co-author and Wolfgang Friederich provided the methods
1180 that generated the tomographic sections. Mark Handy conceived of and prepared the manuscript
1181 with contributions from all co-authors.

1182 **Competing interests** – Mark Handy is a member of the editorial board of this special issue

1183 **Disclaimer** - none

1184 **Special Issue Statement** – this manuscript has been submitted for inclusion in the special issue „New
1185 insights on the tectonic evolution of the Alps and the adjacent orogens“

1186

1187 **Acknowledgements**

1188

1189 We acknowledge the generous funding of the German Science Foundation. (DFG) in the form of
1190 Special Priority Program 2017 “Mountain-Building in Four-Dimensions (4D-MB). This is an arm of the
1191 European “AlpArray” project, which involved the following subprojects: Ha-2403/22-1, Ha-2403/23-1,
1192 Ha-2403/24-1 and FR 1146/12-1. We thank [reviewers Stéphane Guillot and Laurent Jolivet, as well as](#)
1193 [the topical editor, Anne Paul, for critical reviews, despite their disagreement with some of our](#)
1194 [interpretations. Finally, we thank](#) our colleagues in AlpArray for discussions on various topics, some
1195 who were only marginally related to this paper, but all of whom provided a stimulating background
1196 for the ideas presented here: Tobias Diehl, György Hetényi, the late Frank Horvath, Rainer Kind, Edi
1197 Kissling, Eline Le Breton, Frederick Link, Thomas Meier, Jan Pleuger, Georg Rumpker, Wim Spakman,
1198 Frederik Tilmann, Claudia Piromallo, [Othmar Müntener, Phillipe Agard](#), Anne Bernhardt, Vincent
1199 Verwater, Philip Groß, [and](#) Julian Hülscher. A complete list of members of the AlpArray Working
1200 Group can be found here: [http://www.alparray.ethz.ch/en/seismic_network/backbone/data-policy-](http://www.alparray.ethz.ch/en/seismic_network/backbone/data-policy-and-citation/)
1201 [and-citation/](http://www.alparray.ethz.ch/en/seismic_network/backbone/data-policy-and-citation/).

1202

1203

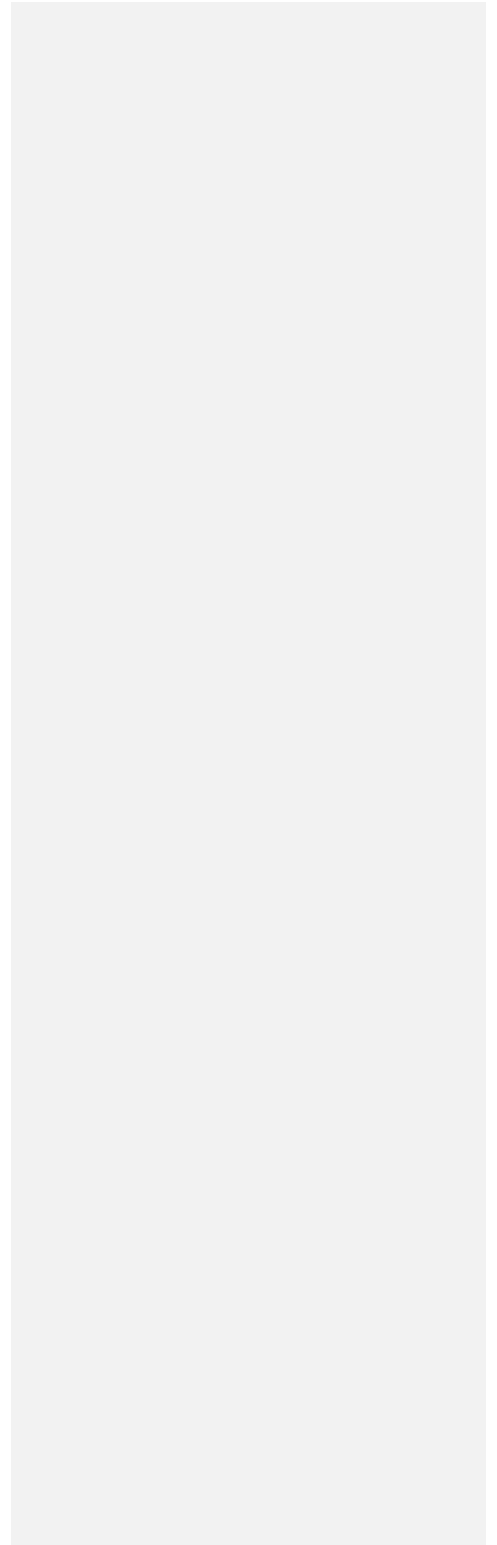
1204

Deleted: research

Deleted: ,

1207

53



1208 **References**

- 1209
1210 Agard, P., and Handy, M.R.: Ocean subduction dynamics in the Alps, in: Shedding Light on the
1211 European Alps, McCarthy, A. and Müntener, O., Guest Editors, Elements [\[2021\]](#) 17, [9-16](#), 2021.
1212 [DOI: 10.2138/gselements.17.1.9](#)
1213
1214 Argand, E.: Des Alpes et de l'Afrique: Bulletin de la Société Vaudoise des Sciences Naturelles, 55,
1215 233–236, 1924.
1216
1217 Artemieva, I.: The Lithosphere: An Interdisciplinary Approach, Cambridge University Press
1218 Monograph, 794 pp., ISBN 9780521843966, 2011.
1219
1220 Babuska, V., Plomerova, J., and Granet, M.: The deep lithosphere in the Alps: a model inferred from P
1221 residuals, Tectonophysics, 176, 137-165, [https://doi.org/10.1016/0040-1951\(90\)90263-8](https://doi.org/10.1016/0040-1951(90)90263-8), 1990.
1222
1223 Baran, R., Friedrich, A. M., and Schlunegger, F.: The late Miocene to Holocene erosion pattern of the
1224 Alpine foreland basin reflects Eurasian slab unloading beneath the western Alps rather than
1225 global climate change, Lithosphere, 6/2, 124–131, doi: 10.1130/L307.1, 2014.
1226
1227 Beccaluva, L., Bianchini, G., Bonadiman, C., Coltorti, M., Milani, L., Salvini, L., Siena, F., and Tassinari,
1228 R.: Intraplate lithospheric and sublithospheric components in the Adriatic domain: Nephelinite
1229 to tholeiite magma generation in the Paleogene Veneto volcanic province, southern Alps,
1230 Geological Society of America Special Paper, 418, 131–152, doi:10.1130/2007.2418(07), 2007.
1231
1232 Behm, M., Brückl, E., Chwatal, W., and Thybo, H.: Application of stacking and inversion techniques
1233 to three-dimensional wide-angle reflection and refraction data of the Eastern Alps, Geophys. J.
1234 Int. 170, 275–298, doi.org/10.1111/j.1365-246X.2007.03393.x, 2007
1235
1236 Bigi, G., Castellarin, A., Catalano, R., Coli, M., Cosentino, D., Dal Piaz, G.V., Lentini, F., Parotto, M.,
1237 Patacca, E., Praturlon, A., Salvini, F., Sartori, R., Scandone, P., and Vai, G.: Synthetic structural
1238 kinematic map of Italy, Sheets 1 and 2, C.N.R., Progetto Finalizzato Geodinamica, SELCA Firenze,
1239 1989.
1240
1241 Bijwaard, H., and Spakman, W.: Non-linear global P-wave tomography by iterated linearized
1242 inversion, Geophys. J. Int., 141,71–82, doi.org/10.1046/j.1365-246X.2000.00053.x, 2000.
1243
1244 Brenker, F.E., and Brey, G.P.: Reconstruction of the exhumation path of the Alpe Arami garnet-
1245 peridotite from depths exceeding 160 km. J. metamorphic Geol., 15, 581-592,
1246 doi/abs/10.1111/j.1525-1314.1997.tb00637.x, 1997.
1247
1248 Brückl, E., Bleibinhaus, F., Gosar, A., et al.: Crustal structure due to collisional and escape tectonics
1249 in the Eastern Alps region based on profiles Alp01 and Alp02 from the ALP 2002 seismic
1250 experiment. J. Geophys. Res. 112, B06308, doi:10.1029/2006JB004687, 2007.
1251
1252 Cammarano, F., Goes, S., Vacher, P., and Giardini, D.: Inferring upper-mantle temperatures from
1253 seismic velocities, Physics of the Earth and Planetary Interiors, 138, 197–222,
1254 doi:10.1016/S0031-9201(03)00156-0, 2003.

Deleted: 1

Formatted: Font: (Default) +Body (Calibri), 12 pt

- 1256
1257 Cassano, E., Anelli, L., Fichera, R., and Cappelli, V.: Pianura Padana: Interpretazione integrate di dati
1258 Geofisici e geologici, 73° Congresso Società Geologica Italiana, Roma, AGIP, 27 pp, 1986.
1259
- 1260 Champagnac, J.D., Molnar, P., Anderson, R.S., Sue, C., and Delacou, B.: Quaternary erosion-induced
1261 isostatic rebound in the western Alps, *Geology*, 35; 195-198, doi: 10.1130/G23053A.1, 2007.
- 1262 Chopin, C.: Coesite and pure pyrope in high-grade blueschists of the Western Alps: a first record and
1263 some consequences, *Contr. Mineral. and Petrol.* 86, 107–118,
1264 <https://doi.org/10.1007/BF00381838>, 1984.
- 1265 Cederbom C.E., van der Beek, P., Schlunegger, F., Sinclair, H.D., and Oncken, O.: Rapid extensive
1266 erosion of the North Alpine foreland basin at 5-4 Ma, *Basin Research*, 23, 528–550, doi:
1267 10.1111/j.1365-2117.2011.00501.x, 2011.
- 1268 Dando B.D.E., Stuart, G.W., Houseman, G.A., Hegedüs, E., Brückl. E., and Radovanovic, S.:
1269 Teleseismic tomography of the mantle in the Carpathian–Pannonian region of central Europe.
1270 *Geophys. J. Int.*, 186, 11–31, doi: 10.1111/j.1365246X.2011.04998.x, 2011.
1271
- 1272 Diehl, T., Husen, S., Kissling, E., and Deichmann, N.: High-resolution 3-D P-wave model of the Alpine
1273 crust, *Geophys. J. Int.*, 179, 1133–1147, doi: 10.1111/j.1365246X.2009.04331.x, 2009.
1274
- 1275 Faccenna, C., Piromallo, C., Crespo-Blanc, A., Jolivet, L., and Rossetti, F.: Lateral slab deformation and
1276 the origin of the western Mediterranean arcs, *Tectonics*, 23, TC1012,
1277 doi:10.1029/2002TC001488, 2004.
1278
- 1279 Favaro S., Handy, M.R., Scharf, A., and Schuster, R.: Changing patterns of exhumation and
1280 denudation in front of an advancing crustal indenter, Tauern Window (Eastern Alps), *Tectonics*,
1281 36, 1053-1071, doi: 10.1002/2016TC004448, 2017.
1282
- 1283 Foulger, G. R., Panza, G. F., Artemieva, I. M., Bastow, I. D., Cammarano, F., Evans, J. R., Hamilton, W.
1284 B., Julian, B. R., Lustrino, M., Thybo, H., and Yanovskaya, T. B.: Caveats on tomographic images,
1285 *Terra Nova*, 25, 259-281, doi: 10.1111/ter.12041, 2013.
1286
- 1287 Fox, M., Herman, F., Kissling E., and Willet, S.D.: Rapid exhumation in the Western Alps driven by
1288 slab detachment and glacial erosion, *Geology*, doi:10.1130/G36411.1, 2015.
1289
- 1290 Fox, M., Herman F., Willett, S.D., and Schmid, S.M.: The exhumation history of the European Alps
1291 inferred from linear inversion of thermochronometric data: *American Journal of Science*, 316,
1292 505-541, doi: 10.2475/06.2016.01, 2016.
1293
- 1294 Franke, W.: The Mid-European segment of the Variscides: tectonostratigraphic units, terrane
1295 boundaries and plate tectonics evolution, *Geological Society, London, Special Publications*, 179,
1296 35-61, <https://doi.org/10.1144/GSL>, 2000.
1297
- 1298 Franke, W., Cock, L.R.M., and Torsvik, T.H.: The Palaeozoic Variscan oceans revisited. *Gondwana*
1299 *Research*, 48, 257-284, <http://dx.doi.org/10.1016/j.gr.2017.03.005>, 2017.

1300
1301 Fügenschuh, B., Seward, D., and Mancktelow, N.S.: Exhumation in a convergent orogen: the western
1302 Tauern Window. *Terra Nova*, 9, 213–217, doi: 10.1111/j.1365-3121.1997.tb00015.x, 1997
1303
1304 Geissler, W.H., Sodoudi, F., and Kind, R.: Thickness of the central and eastern European lithosphere
1305 as seen by S receiver functions: *Geophysical Journal International*, 181, 604–634, doi:
1306 10.1111/j.1365-246X.2010.04548.x, 2010.
1307
1308 Genser, J., Cloetingh, S. A. L., and Neubauer, F.: Late orogenic rebound and oblique Alpine
1309 convergence: New constraints from subsidence analysis of the Austrian Molasse basin, *Global
1310 and Planetary Change*, 58, 1–4, 214–223, doi: 10.1016/j.gloplacha.2007.03.010, 2007.
1311
1312 Giacomuzzi, G., Chiarabba, C., and De Gori, P.: Linking the Alps and Apennines subduction systems:
1313 New constraints revealed by high-resolution teleseismic tomography. *Earth and Planetary
1314 Science Letters*, 301, 531–543, doi:10.1016/j.epsl.2010.11.033, 2011.
1315
1316 Giacomuzzi, G., Civalleri, M., DeGori, P., and Chiarabba, C.: A 3D Vs model of the upper mantle
1317 beneath Italy: Insight on the geodynamics of central Mediterranean, *Earth and Planetary
1318 Science Letters*, 335-336, 105-120, doi.org/10.1016/j.epsl.2012.05.004, 2012.
1319
1320 Goes, S., Govers, R., and Vacher, P.: Shallow mantle temperatures under Europe from P and S wave
1321 tomography: *Journal of Geophysical Research* 105/B5, 11153-11169,
1322 doi.org/10.1029/1999JB900300, 2000.
1323
1324 Grad, M., Tiira, T., and ESC Working Group: The Moho depth map of the European Plate. *Geophys. J.
1325 Int.* 176, 279–292, doi: 10.1111/j.1365-246X.2008.03919.x, 2009.
1326
1327 Grenerczy, G., Sella, G., Stein, S., Kenyeres, A.: Tectonic implications of the GPS velocity field in the
1328 northern Adriatic region, *Geophysical Research Letters*, 32, doi:10.1029/2005GL022947, 2005.
1329
1330 Gross, P., Handy, M. R., John, T., Pestal, G., and Pleuger, J.: Crustal-scale sheath folding at HP
1331 conditions in an exhumed Alpine subduction zone (Tauern Window, Eastern Alps), *Tectonics*,
1332 39, doi.org/10.1029/2019TC005942, 2020.
1333
1334 Grunert, P., Hinsch, R., Sachsenhofer, R. F., Bechtel, A., Ćorić, S., Harzhauser, M., Piller, W.E., and
1335 Sperl, H.: Early Burdigalian infill of the Puchkirchen Trough (North Alpine Foreland Basin,
1336 Central Paratethys): Facies development and sequence stratigraphy. *Marine and Petroleum
1337 Geology*, 39/1, 164–186, doi: 10.1016/j.marpetgeo.2012.08.009, 2013.
1338
1339 Hammond, J. O. S.: Constraining melt geometries beneath the Afar Depression, Ethiopia from
1340 teleseismic receiver functions: The anisotropic H-κ stacking technique, *Geochem. Geophys.
1341 Geosyst.*, 15, 1316–1332, doi:10.1002/2013GC005186, 2014
1342
1343 Handy, M. R., Schmid, S. M., Bousquet, R., Kissling, E., and Bernoulli, D.: Reconciling plate-tectonic
1344 reconstructions with the geological-geophysical record of spreading and subduction in the Alps,
1345 *Earth Science Reviews*, 102, 121-158, doi:10.1016/j.earscirev.2010.06.002, 2010.
1346

1347 Handy, M. R., Ustaszewski, K., and Kissling, E.: Reconstructing the Alps–Carpathians–Dinarides as a
 1348 key to understanding switches in subduction polarity, slab gaps and surface motion, *Int. J. Earth*
 1349 *Sci. (Geol. Rundsch.)*, 104,1–26 doi, 10.1007/s00531-014-1060-3, 2015.
 1350
 1351 Hetényi, G. Molinari, I., Clinton, J., Bokelmann, G., Bondár, I., Crawford, W.C., Dessa, J.X., Doubre, C.,
 1352 Friederich, W., Fuchs, F., Giardini, D., Grácz, Z., Handy, M.R., Herak, M., Jia, Y., Kissling, E.,
 1353 Kopp, H., Korn, M., Margheriti, L., Meier, T., Mucciarelli, M., Paul, A., Pesaresi, D., Piromallo, C.,
 1354 Plenefisch, Th., Plomerová, J., Ritter, J., Rumpker, G., Šipka, V., Spallarossa, D., Thomas, Ch.,
 1355 Tilmann, F., Wassermann, J., Weber, M., Wéber, Z., Wetzergom, V., Živčić, M., and AlpArray
 1356 Seismic Network Team , AlpArray OBS Cruise Crew, AlpArray Working Group: The AlpArray
 1357 Seismic Network: A large-scale European experiment to image the Alpine orogen. *Surveys in*
 1358 *Geophysics*, 39, 1009-1033, doi.org/10.1007/s10712-018-9472-4, 2018.
 1359
 1360 Hinsch, R.: Laterally varying structure and kinematics of the Molasse fold and thrust belt of the
 1361 Central Eastern Alps: Implications for exploration, *AAPG Bulletin*, 97, 10, 1805–1831.
 1362 doi:10.1306/04081312129, 2013.
 1363
 1364 Horváth, F., Bada, G., Szafian, P., Tari, G., Adam, A. and Cloetingh, S.: Formation and deformation of
 1365 the Pannonian Basin: constraints from observational data. In: Gee, D. G. & Stephenson, R. A.
 1366 (eds), *European Lithosphere Dynamics*, Geological Society London Memoirs, 32, 191–206,
 1367 doi.org/10.1144/GSL.MEM.2006.032.01.11, 2006.
 1368
 1369 Horváth, F., Musitz, B., Balázs, A., Végh, A., Uhrin, A., Nádor, A., Koroknai, B., Pap, N., Tóth, T., and
 1370 Wórum, G.: Evolution of the Pannonian basin and its geothermal resources. *Geothermics*, 53,
 1371 328–352, doi.org/10.1016/j.geothermics.2014.07.009, 2015.
 1372
 1373 Jolivet, L., Faccenna, C., and Piromallo, C.: From mantle to crust: Stretching the Mediterranean,
 1374 *Earth and Planetary Science Letters*, 285, 1–2, 198–209.
 1375 https://doi.org/10.1016/j.epsl.2009.06.017, 2009.
 1376
 1377 Jones, A., G., Plomerova, J., Korja, T., Sodoudi, F., and Spakman, W.: Europe from the bottom up: A
 1378 statistical examination of the central and northern European lithosphere–asthenosphere
 1379 boundary from comparing seismological and electromagnetic observations, *Lithos*, 120, 14–29,
 1380 doi:10.1016/j.lithos.2010.07.013, 2010.
 1381
 1382 Jordan, T.H.: The Continental Tectosphere, *Reviews of Geophysics and Space Physics*, 13/3,
 1383 doi.org/10.1029/RG013i003p00001, 1975.
 1384
 1385 Jordan, T.H.: Continents as a chemical boundary layer, *Phil. Trans. R. Soc. Lond.*, A 301, 359–373,
 1386 1981.
 1387
 1388 Karato, S., and Jung, H.: Water, partial melting and the origin of the seismic low velocity and high
 1389 attenuation zone in the upper mantle, *Earth and Planetary Science Letters*, 157, 193–207, 1998.
 1390
 1391 Karousová, H., Babuška, V., and Plomerová, J.: Upper-mantle structure beneath the southern
 1392 Bohemian Massif and its surroundings imaged by high-resolution tomography, *Geophys. J. Int.*,
 1393 194, 1203–1215, https://doi.org/10.1093/gji/ggt159, 2013.

1394
1395 Kastelic, V., Vrabec, M., Cunningham, D., and Gosar, A.: Neo-Alpine structural evolution and
1396 present-day tectonic activity of the eastern Southern Alps: The case of the Ravne Fault, NW
1397 Slovenia, *Journal of Structural Geology*, 30, 963-975, doi:10.1016/j.jsg.2008.03.009, 2008.
1398
1399 Kästle, E.D., Rosenberg, C., Boschi, L., Bellahsen, N., Meier, T., El-Sharkawy, A.: Slab break-offs in
1400 the Alpine subduction zone. *Int. J. Earth Sci. (Geol Rundsch)*, 109, 587–603,
1401 <https://doi.org/10.1007/s00531-020-01821-z>, 2020.
1402
1403 Kind, R., Schmid, S. M., Yuan, X., Heit, B., Meier, T., and the AlpArray and AlpArray-SWATH-D
1404 Working Groups: Moho and uppermost mantle structure in the greater Alpine area from S-to-P
1405 converted waves, *Solid Earth*, this volume, 2021.
1406
1407 Király, Á., Faccenna, C., and Funicello, F.: Subduction zones interaction around the Adria microplate
1408 and the origin of the Apenninic arc: *Tectonics*, 37, 3941–3953,
1409 <https://doi.org/10.1029/2018TC00521>, 2018.
1410
1411 Kissling, E., and Schlunegger, F.: Rollback orogeny model for the evolution of the Swiss Alps,
1412 *Tectonics*, 37, doi.org/10.1002/2017TC004762, 2018.
1413
1414 Kissling, E., Schmid, S. M., Lippitsch, R., Ansorge, J., and Fügenschuh, B.: Lithosphere structure and
1415 tectonic evolution of the Alpine arc: new evidence from high-resolution teleseismic
1416 tomography, *Geological Society of London Memoirs*, 32, 129-145,
1417 doi.org/10.1144/GSL.MEM.2006.032.01.08, 2006.
1418
1419 Koulakov, I., Kaban, M., Tesauro, M., and Cloetingh, S.: P-and S-velocity anomalies in the upper
1420 mantle beneath Europe from tomographic inversion of ISC data, *Geophys. J. Int.*, 179, 345–366,
1421 doi: 10.1111/j.1365-246X.2009.04279.x, 2009.
1422
1423 Kuhlemann, J., and Kempf, O.: Post-Eocene evolution of the North Alpine Foreland Basin and its
1424 response to Alpine tectonics, *Sedimentary Geology*, 152, 45–78, doi.org/10.1016/S0037-
1425 0738(01)00285-8, 2002.
1426
1427 Kurz, W., Handler, R., and Bertoldi, C.: Tracing the exhumation of the Eclogite Zone (Tauern
1428 Window, Eastern Alps) by ⁴⁰Ar/³⁹Ar dating of white mica in eclogites, *Swiss J. Geosci.* 101,
1429 Supplement 1, S191–S206, 10.1007/s00015-008-1281-1, 2008.
1430
1431 Le Breton, E., Brune, S., Ustaszewski, K., Zahirovic, S., Seton, M., and Müller, R. D.: Kinematics and
1432 extent of the Piemont-Liguria Basin – implications for subduction processes in the Alps, *Solid*
1433 *Earth*, <https://doi.org/10.5194/se-2020-161>, 2021.
1434
1435 Lippitsch, R., Kissling, E., and Ansorge, J.: Upper mantle structure beneath the Alpine orogen from
1436 high-resolution teleseismic tomography, *J. Geophys. Res.*, 108(B8), 2376,
1437 doi:10.1029/2002JB002016, 2003.
1438

1439 Lyu, C., Pedersen, H.A., Paul, A., Zhao, L., Solarino, S., and CIFALPS Working Group: Shear wave
1440 velocities in the upper mantle of the Western Alps: new constraints using array analysis of
1441 seismic surface waves. *Geophys. J. Int.* (2017) 210, 321–331, 2017. doi: 10.1093/gji/ggx166.
1442

1443 Macera, P., Gasperini, D., Piromallo, C., Blichert-Toft, J., Bosch, D., Del Moro, A., and Martin, S.:
1444 Geodynamic implications of deep mantle upwelling in the source of Tertiary volcanics from the
1445 Veneto region (South-Eastern Alps), *Journal of Geodynamics*, 36, 563–590,
1446 doi:10.1016/j.jog.2003.08.004, 2003.
1447

1448 Macera, P., Gasperini, D., Ranalli, G., and Mahatsente, R.: Slab detachment and mantle plume
1449 upwelling in subduction zones: an example from the Italian South-Eastern Alps, *Journal of
1450 Geodynamics*, 45, 32–48, doi:10.1016/j.jog.2007.03.004, 2008.
1451

1452 Maffione, M., Speranza, F., Faccenna, C., Cascella, A., Vignaroli, G., and Sagnotti, L.: A synchronous
1453 Alpine and Corsica-Sardinia rotation: *Journal of Geophysical Research*, 113, B03104,
1454 doi:10.1029/2007JB005214, 2008.
1455

1456 Malusà, M. G., Frezzotti, M. L., Ferrando, S., Brandmayr, E., Romanelli, F., and Panza, G. F.: Active
1457 carbon sequestration in the Alpine mantle wedge and implications for long-term climate trends.
1458 *Scientific Reports*, 8(1), 1–8, 2018.
1459

1460 Malusà, M. G., Guillot, S., Zhao, L., Paul, A., Solarino, S., Dumont, T., Schwartz, S., Aubert, C.,
1461 Baccheschi, P., Eva, E., Lu, Y., Lyu, C., Pondrelli, S., Salimbeni, S., Sun, W. and Yuan, H.: The deep
1462 structure of the Alps based on the CIFALPS seismic experiment: A synthesis. *Geochemistry,
1463 Geophysics, Geosystems*, 22, e2020GC009466. <https://doi.org/10.1029/2020GC009466>
1464

1464 Márton, E., Grabowski, J., Tokarski, A.K., and Túnyi, I.: Palaeomagnetic results from the fold and
1465 thrust belt of the Western Carpathians: an overview, *Geological Society, London, Special
1466 Publications*, 425, 7-36, <https://doi.org/10.1144/SP425.1>, 2015.

1467 Matenco, L., and Radivojević, D.: On the formation and evolution of the Pannonian Basin:
1468 Constraints derived from the structure of the junction area between the Carpathians and
1469 Dinarides, *Tectonics*, 31, TC6007, doi:10.1029/2012TC003206, 2012.

1470 Matte, P.: Tectonics and plate tectonics model for the Variscan belt of Europe. *Tectonophysics*, 126,
1471 2–4, 15, 329-332, 335-344, 347-374. [https://doi.org/10.1016/0040-1951\(86\)90237-4](https://doi.org/10.1016/0040-1951(86)90237-4). 1986.
1472

1473 Mazur, S., Aleksandrowski, P., Gągała, Ł., Krzywiec, P., Żaba, J., Gaidzik, K., and Sikora, R.: Late
1474 Palaeozoic strike-slip tectonics versus oroclinal bending at the SW outskirts of Baltica: case of
1475 the Variscan belt's eastern end in Poland, *International Journal of Earth Sciences*, 109, 1133-
1476 1160, doi:10.1007/s00531-019-01814-7, 2020.
1477

1478 Mey, J., Scherler, D., Wickert, A. D., Egholm, D. L., Tesauro, M., Schildgen, T. F., and Strecker M. R.:
1479 Glacial isostatic uplift of the European Alps, *Nature Communications*, 7: 13382,
1480 doi:10.1038/ncomms13382, 2016.
1481

Formatted: Font: Not Bold

1482 Mitchell, B.J.: Anelastic structure and evolution of the continental crust and upper mantle from
1483 seismic surface wave attenuation, *Reviews of Geophysics*, 33, 441-462,
1484 <https://doi.org/10.1029/95RG02074>
1485

1486 Mitterbauer, U., Behm, M., Brückl, E., Lippitsch, R., Guterch, A., Keller, G. R., Koslovskaya, E.,
1487 Rumpfhuber, E. M., and Šumanovac, F.: Shape and origin of the East-Alpine slab constrained by
1488 the ALPASS teleseismic model, *Tectonophysics* 510, 195–206, doi:10.1016/j.tecto.2011.07.001,
1489 2011.
1490

1491 Molli, G., Crispini, L., Mosca, P., Piana, P., and Federico, L.: Geology of the Western Alps-Northern
1492 Apennine junction area: a regional review. *Journal of the Virtual Explorer*, 36/9, 1-49,
1493 doi:10.3809/jvirtex.2010.00215, 2010.
1494

1495 Molli, G., Brogi, A., Caggianelli, A., Capezzuoli, E., Liotta, D., Spina, A., and Zibra, I.: Late Palaeozoic
1496 tectonics in Central Mediterranean: a reappraisal, *Swiss Journal of Geosciences*, 113,
1497 doi.org/10.1186/s00015-020-00375-1, 2020.
1498

1499 Munzerová, H., Plomerová, J., and Kissling, E.: Novel anisotropic teleseismic body-wave tomography
1500 code AniTomo to illuminate heterogeneous anisotropic upper mantle: Part I —Theory and
1501 inversion tuning with realistic synthetic data. *Geophys. J. Int.* (2018) 215, 524–545, doi:
1502 10.1093/gji/ggy296, 2018.
1503

1504 [Müntener, O., Ulmer, P., Blundy, J.D., Superhydrous Arc Magmas in the Alpine Context. Elements, in:](#)
1505 [Shedding Light on the European Alps, McCarthy, A. and Müntener, O., Guest Editors, Elements](#)
1506 [\(2021\) 17, 35-40, DOI: 10.2138/gselements.17.1.35](#)
1507

1508 Nagel, T. J., Herwartz, D., Rexroth, S., Münker, C., Froitzheim, N., and Kurz, W.: Lu-Hf dating,
1509 petrography, and tectonic implications of the youngest Alpine eclogites (Tauern Window,
1510 Austria), *Lithos*, 170, 179–190, <https://doi.org/10.1016/j.lithos.2013.02.008>, 2013.
1511

1512 Nussbaum, C.: Neogene tectonics and thermal maturity of sediments of the easternmost Southern
1513 Alps (Friuli are, Italy), unpublished PhD thesis Université de Neuchâtel, Switzerland, 2000.
1514

1515 Paffrath, M. H., Friederich, W., and AlpArray & AlpArray-SWATH D Working Groups: Teleseismic P-
1516 waves at the AlpArray seismic network: Wave fronts, absolute traveltimes and traveltime
1517 residuals, *Solid Earth*, <https://doi.org/10.5194/se-2020-189>, this volume, 2021a.
1518

1519 Paffrath, M. H., Friederich, W., Schmid, S.M., Handy, M.R. and AlpArray & AlpArray-SWATH D
1520 Working Groups: Teleseismic traveltime tomography of the greater Alpine region. *Solid Earth*,
1521 this volume, 2021b.
1522

1523 Perry, H. K. C., Jaupart, C., Mareschal, J.-C., and Shapiro, N. M.: Upper mantle velocity-temperature
1524 conversion and composition determined from seismic refraction and heat flow, *J. Geophys.*
1525 *Res.*, 111, B07301, doi:10.1029/2005JB003921, 2006.
1526

1527 Pfiffner, O.A., Lehner, P., Heitzmann, P., Mueller, St., and Steck, A. (Eds.) : Deep Structure of the
1528 Swiss Alps: Results of NRP 20: Birkhäuser et al., Basel, 460pp., ISBN 3-7643 5254 X, 1997.

Formatted: English (US)

Formatted: Font: (Default) +Body (Calibri), 12 pt

Formatted: Font: (Default) +Body (Calibri), 12 pt

Formatted: Font: (Default) +Body (Calibri), 12 pt

Formatted: Font colour: White

Formatted: English (US)

Formatted: Indent: Left: 0 cm

1529
1530 Pfiffner, O. A., and Hitz, L.: Geologic interpretation of the seismic profiles in the Eastern Traverse
1531 (lines E1 – E3, E7-E9): eastern Alps, Chapter 9 in Pfiffner et al. (Eds.) Deep Structure of the Alps:
1532 Results of NRP 20, Birkhäuser et al., Basel, 73-100, 1997.
1533
1534 Picotti, V., and Pazzaglia, F. J.: A new active tectonic model for the construction of the Northern
1535 Apennines mountain front near Bologna (Italy), *J. Geophys. Res.*, 113, B08412,
1536 doi:10.1029/2007JB005307, 2008.
1537
1538 Piromallo, C., and Morelli, A.: P wave tomography of the mantle under the Alpine-Mediterranean
1539 area. *J. Geophys. Res.*, 108(B2), 2065, doi:10.1029/2002JB001757, 2003.
1540
1541 Pomella, H., Klötzli, U., Scholger, R., Stipp, M., and Fügenschuh, B.: The Northern Giudicarie and the
1542 Meran-Mauls fault (Alps, Northern Italy) in the light of new paleomagnetic and
1543 geochronological data from boudinaged Eo-Oligocene tonalites, *Int. J. Earth Sci.*, 100, 1827–
1544 1850, doi:10.1007/s00531-010-0612-4, 2011.
1545
1546 Pomella H, Stipp M, and Fügenschuh, B.: Thermochronological record of thrusting and strike-slip
1547 faulting along the Giudicarie fault system (Alps, Northern Italy). *Tectonophysics*, 79:118–130,
1548 2012.
1549
1550 Qorbani, E., Bianchi, I., and Bokelmann, G.: Slab detachment under the Eastern Alps seen by seismic
1551 anisotropy, *Earth and Planetary Science Letters*, 409, 96-108,
1552 doi.org/10.1016/j.epsl.2014.10.049, 2015.
1553
1554 Ratschbacher, L., Frisch, W., Linzer, H.-G., and Merle, O.: Lateral extrusion in the Eastern Alps, part
1555 2: Structural analysis. *Tectonics*, 10(2), 257–271 <https://doi.org/10.1029/90TC02623>, 1991.
1556
1557 Ratschbacher, L., Dingeldey, C., Miller, C., Hacker, B. R., and McWilliams, M. O.: Formation,
1558 subduction, and exhumation of Penninic oceanic crust in the Eastern Alps: Time constraints
1559 from 40 Ar/39 Ar geochronology, *Tectonophysics*, 394(3), 155–170,
1560 <https://doi.org/10.1016/j.tecto.2004.08.003>, 2004.
1561
1562 Rawlinson, N., and Sambridge, M.: The Fast Marching Method: An Effective Tool for Tomographic
1563 Imaging and Tracking Multiple Phases in Complex Layered Media, *Exploration Geophysics*, 36:4,
1564 341-350, doi:10.1071/EG05341, 2005.
1565
1566 Rawlinson, N., Reading, A. M., and Kennett, B. L. N.: Lithospheric structure of Tasmania from a novel
1567 form of teleseismic tomography, *J. Geophys. Res.*, 111, B02301, doi:10.1029/2005JB003803,
1568 2006.
1569
1570 Rosenberg, C. L.: Shear zones and magma ascent: A model based on a review of the Tertiary
1571 magmatism in the Alps, *Tectonics*, 23, TC3002, doi:10.1029/2003TC001526, 2004.
1572
1573 Rosenberg, C.L., and Kissling, E.: Three-dimensional insight into Central-Alpine collision: Lower plate
1574 or upper-plate indentation?, *Geology*, 41/12, 1219–122, doi:10.1130/G34584.1, 2013.
1575

1576 Rosenberg, C. L., Schneider, S., Scharf, A., Bertrand, A., Hammerschmidt, K., Rabaute, A., and Brun,
1577 J.-P.: Relating collisional kinematics to exhumation processes in the Eastern Alps, *Earth-Science*
1578 *Reviews*, 176, 311–344, doi.org/10.1016/j.earscirev.2017.10.013, 2018.

1579
1580 Scharf, A., Handy, M.R., Favaro, S., Schmid, S.M., and Bertrand, A.: Modes of orogen-parallel
1581 stretching and extensional exhumation in response to microplate indentation and roll-back
1582 subduction (Tauern Window, Eastern Alps), *International Journal of Earth Sciences*, 102, 1627-
1583 1654, doi.10.1007/s00531-013-0894-4, 2013.

1584
1585 Schefer, S., Cvetković, V., Fügenschuh, B., Kounov, A., Ovtcharova, M., Schaltegger, U., Schmid, S.
1586 M.: Cenozoic granitoids in the Dinarides of southern Serbia: age of intrusion, isotope
1587 geochemistry, exhumation history and significance for the geodynamic evolution of the Balkan
1588 Peninsula, *Int. J. Earth Sci.* 100, 1181-1206, https://doi.org/10.1007/s00531-010-0599-x, 2011.

1589
1590 Schertl, H.-P., Schreyer, W., and Chopin, C.: The pyrope-coesite rocks and their country rocks at
1591 Parigi, Dora Maira Massif, Western Alps: detailed petrography, mineral chemistry and PT-path
1592 *Contrib. Mineral. Petrol.* 108, 1-21, 1991

1593
1594 Schmid, S. M., Pfiffner, O. A., Froitzheim, N., Schönborn, G., and Kissling, E.: Geophysical-geological
1595 transect and tectonic evolution of the Swiss-Italian Alps, *Tectonics*, 15, 1036-1064,
1596 doi.10.1029/96TC00433, 1996.

1597
1598 Schmid, S. M., Fügenschuh, B., Kissling, E., and Schuster, R.: Tectonic map and overall architecture of
1599 the Alpine orogen. *Eclogae geologicae Helvetiae* 97, 93-117, doi.org/10.1007/s00015-004-1113-
1600 x, 2004.

1601
1602 Schmid, S. M., Bernoulli, D., Fügenschuh, B., Matenco, L., Schefer, S., Schuster, R., Tischler, M., and
1603 Ustaszewski, K.: The Alpine-Carpathian-Dinaridic orogenic system: correlation and evolution of
1604 tectonic units. *Swiss Journal of Geosciences*, 101, 139-183, doi:10.1007/s00015-008-1247-3,
1605 2008.

1606
1607 Schmid, S. M., Scharf, A., Handy, M. R., and Rosenberg, C. L.: The Tauern Window (Eastern Alps,
1608 Austria): a new tectonic map, with cross-sections and a tectonometamorphic synthesis. *Swiss*
1609 *Journal of Geosciences*, 106, 1-32, doi. 10.1007/s00015-013-0123-y, 2013.

1610
1611 Schmid, S. M., Kissling, E., Diehl, T., van Hinsbergen D. J. J., and Molli, G.: Ivrea mantle wedge, arc of
1612 the Western Alps, and kinematic evolution of the Alps–Apennines orogenic system, *Swiss*
1613 *Journal of Geosciences*, 110, 581-612, doi.10.1007/s00015-016-0237-0, 2017.

1614
1615 Schönborn, G.: Alpine tectonics and kinematic models of the central Southern Alps, *Mem. Sci. Geol.*
1616 *Padova*, 44, 229–393, 1992.

1617
1618 Schönborn, G.: Balancing cross sections with kinematic constraints: The Dolomites (northern Italy),
1619 *Tectonics* 18, 527–545, doi.org/10.1029/1998TC900018, 1999.

1620
1621 Schulmann, K., Lexa, O., Vojtech J., Lardeaux, J. M., and Edel, J. B.: Anatomy of a diffuse cryptic
1622 suture zone: An example from the Bohemian Massif, *European Variscides*, *Geology*, 42, 275–

1623 278, doi:10.1130/G35290.1, 2014.

1624

1625 Seghedi, I., and Downes, H.: Geochemistry and tectonic development of Cenozoic magmatism in the

1626 Carpathian–Pannonian region, *Gondwana Research*, 20, 655–672, doi:10.1016/j.gr.2011.06.009,

1627 2011.

1628

1629 Seghedi, I., Ersoy, Y.E., and Helvacı, C.: Miocene–Quaternary volcanism and geodynamic evolution in

1630 the Pannonian Basin and the Menderes Massif: A comparative study, *Lithos* 180–181, 25–42,

1631 doi.org/10.1016/j.lithos.2013.08.017, 2013.

1632

1633 Serpelloni, E., Vannucci, G., Anderlini, L., and Bennett, R. A.: Kinematics, seismotectonics and

1634 seismic potential of the eastern sector of the European Alps from GPS and seismic deformation

1635 data, *Tectonophysics* 688, 157–181, dx.doi.org/10.1016/j.tecto.2016.09.026, 2016.

1636

1637 Serretti, P., and Morelli, A.: Seismic rays and traveltimes tomography of strongly heterogeneous

1638 mantle structure: application to the Central Mediterranean, *Geophys. J. Int.*, 187, 1708–1724,

1639 doi: 10.1111/j.1365-246X.2011.05242.x, 2011.

1640

1641 Shito, A., Karato, S., Matsukage, K., N., and Nishihara Y.: Towards Mapping the Three-Dimensional

1642 Distribution of Water in the Upper Mantle from Velocity and Attenuation Tomography,

1643 *Geophysical Monograph*, 168, 225–236, DOI: 10.1029/168GM17, 2006.

1644

1645 Singer, J., Diehl, T., Husen, S., Kissling, E., and Duretz, T.: Alpine lithosphere slab rollback causing

1646 lower crustal seismicity in northern foreland, *Earth and Planetary Science Letters*, 397, 42–56,

1647 doi.org/10.1016/j.epsl.2014.04.002, 2014.

1648

1649 Smye, A. J., Bickle, M. J., Holland, T. J. B., Parrish, R. R., and Condon, D. J.: Rapid formation and

1650 exhumation of the youngest Alpine eclogites: A thermal conundrum to Barrovian

1651 metamorphism, *Earth and Planetary Science Letters*, 306(3–4), 193–204, https://doi.

1652 org/10.1016/j.epsl.2011.03.037, 2011.

1653

1654 Spada, M., Bianchi, I., Kissling, E., Piana Agostinetti, N., and Wiemer, S.: Combining controlled-

1655 source seismology and receiver function information to derive 3-D Moho topography for Italy,

1656 *Geophys. J. Int.*, 194, 1050–1068, doi: 10.1093/gji/ggt148, 2013.

1657

1658 Spakman, W., and Wortel, M.J.R.: Tomographic View on Western Mediterranean Geodynamics, in:

1659 *The TRANSMED Atlas, The Mediterranean Region from Crust to Mantle*, edited by: Cavazza, W.

1660 et al., Springer, Berlin, Heidelberg, 31–52, https://doi.org/10.1007/978-3-642-18919-7_2, 2004.

1661

1662 Speranza, F., Villa, I.M., Sagnotti, L., Florindo, F., Cosentino, D., Cipollari, P., and Mattei, M.: Age of

1663 the Corsica–Sardinia rotation and Liguro–Provençal Basin spreading: new paleomagnetic and

1664 Ar/Ar evidence, *Tectonophysics*, 231–251, https://doi.org/10.1016/S0040-1951(02)00031-8,

1665 2002.

1666

1667 Stipčević, J., Tkalčić, H., Herak, M., Markušić, S., and Herak, D.: Crustal and uppermost mantle

1668 structure beneath the External Dinarides, Croatia, determined from teleseismic receiver

1669 functions, *Geophysical Journal International*, 185(3), 1103–1119. doi:10.1111/j.1365-
 1670 246x.2011.05004.x, 2011.
 1671
 1672 Stipčević, J., Herak, M., Molinari, I., Dasović, I., Tkalčić, H., & Gosar, A.: Crustal thickness beneath the
 1673 Dinarides and surrounding areas from receiver functions, *Tectonics*, 37,
 1674 doi.org/10.1029/2019TC005872, 2020.
 1675
 1676 Sun, W., Zhao, L., Malusà, M.G., Guillot, S., Fu, L.-Y.: 3-D Pn tomography reveals continental
 1677 subduction at the boundaries of the Adriatic microplate in the absence of a precursor oceanic
 1678 slab. *Earth and Planetary Science Letters* 510, 131–141, 2019.
 1679 https://doi.org/10.1016/j.epsl.2019.01.012
 1680
 1681 Tesauro, M., Kaban, M. K., and Cloetingh, S. A. P. L.: EuCRUST-07: A new reference model for the
 1682 European crust, *Geophysical Research Letters*, 35(5), doi:10.1029/2007gl032244, 2008.
 1683
 1684 Ustaszewski, K., Schmid, S. M., Fügenschuh, B., Tischler, M., Kissling, E., and Spakman, W.: A map-
 1685 view restoration of the Alpine–Carpathian–Dinaridic system for the Early Miocene, *Swiss J.*
 1686 *Geosci.*, 101, 273–294, doi: 10.1007/s00015-008-1288-7, 2008.
 1687
 1688 Verwater, V. F., Le Breton, E., Handy, M. R., Picotti, V., Najafabadi, A.J., Haberland, C.: Neogene
 1689 kinematics of the Giudicarie Belt and eastern Southern Alpine orogenic front (Northern Italy),
 1690 *Solid Earth*, doi: org/10.5194/se-2021-19, 2021, this volume.
 1691
 1692 van der Meer, D. G., Spakman, W., van Hinsbergen, D. J. J., Amaru, M. L., and Torsvik, T. H.:
 1693 Towards absolute plate motions constrained by lower-mantle slab remnants. *Nat. Geosci.*
 1694 3, 36–40, 2010.
 1695
 1696 van der Meer, D. G., van Hinsbergen, D. J. J., and Spakman, W.: Atlas of the underworld: Slab
 1697 remnants in the mantle, their sinking history, and a new outlook on lower mantle viscosity,
 1698 *Tectonophysics*, 723, 309–448, doi.org/10.1016/j.tecto.2017.10.004, 2018.
 1699
 1700 van Hinsbergen, D. J. J., Torsvik, T. H., Schmid, S. M., Matenco, L. C., Maffione, M., Vissers, R. L .M.,
 1701 Gürer, D., and Spakman, W.: Orogenic architecture of the Mediterranean region and kinematic
 1702 reconstruction of its tectonic evolution since the Triassic. *Gondwana Research* 81, 79-229,
 1703 https://doi.org/10.1016/j.gr.2019.07.009, 2020.
 1704
 1705 von Blanckenburg, F., and Davies, J. H.: Slab breakoff: A model for syncollisional magmatism and
 1706 tectonics in the Alps, *Tectonics*, 14, 120-131, doi.org/10.1029/94TC0205, 1995.
 1707
 1708 Waldhauser, F., Lippitsch, R., Kissling, E., and Ansorge, J.: High-resolution teleseismic tomography of
 1709 upper-mantle structure using an a priori three-dimensional crustal model, *Geophysical Journal*
 1710 *International*, 150, 403–414, doi.org/10-1046/j.1365-246X.2002.01690.x, 2002.
 1711
 1712 Wortel, M., J., R., and Spakman, W.: Subduction and Slab Detachment in the Mediterranean-
 1713 Carpathian Region: *Science*, 290, 1910-1917, doi: 10.1126/science.290.5498.1910, 2000.
 1714

1715 Zahorec, P., Papčo, J., Pašteka, R., Bielik, M., Bonvalot, S., Braitenberg, C., Ebbing, J., Gabriel, G.,
1716 Gosar, A., Grand, A., Götze, H.-J., Hetényi, G., Holzrichter, N., Kissling, E., Marti, U., Meurers, B.,
1717 Mrlina, J., Nogová, E., Pastorutti, A., Salaun, C., Scarponi, M., Sebera, J., Seoane, L., Skiba, P., Szűcs,
1718 E., and Varga, M.: The first pan-Alpine surface-gravity database, a modern compilation that crosses
1719 frontiers. *Earth Syst. Sci. Data*, 13, 2165–2209, 2021, <https://doi.org/10.5194/essd-13-2165-2021>
1720
1721 Zhao, L., Paul, A., Guillot, S., Solarino, S., Malusá, M., Zheng, T., Aubert, C., Dumont, T., Schwartz, S.,
1722 Zhu, R., Wang, Q.: First seismic evidence for continental subduction beneath the Western Alps.
1723 *Geology*, 43; 9, 815–818, 2015. doi:10.1130/G36833.1
1724
1725 Zhao, L., Paul, A., Malusà, M. G., Xu, X., et. al.: Continuity of the Alpine slab unraveled by high-
1726 resolution P wave tomography, *Journal of Geophysical Research, Solid Earth*, 121(12), 8720–
1727 8737, doi:10.1002/2016jb013310, 2016.
1728
1729